Counteracting contribution of the Upper and Lower Meridional Overturning Limbs to the North Atlantic Nutrient Budgets: enhanced imbalance in 2010

L.I. Carracedo[1,2], H. Mercier[1], E. McDonagh[2,3], G. Rosón[4], R. Sanders[2,3], C.M. Moore[5], S. Torres-Valdés[6], P. Brown[2], P. Lherminier[1], F.F. Pérez[7]

[1] University of Brest, CNRS, Ifremer, IRD, Laboratoire d'Océanographie Physique et Spatiale (LOPS), IUEM, Centre Ifremer de Bretagne, F-29280, Plouzané, France.
[2] National Oceanography Centre (NOC), Southampton SO14 3ZH, UK.
[3] NORCE Norwegian Research Centre, Bjerknes Centre for Climate Research, Bergen, Norway.
[4] Faculty of Marine Sciences, University of Vigo, Campus Lagoas-Marcosende, 36200 Vigo, Spain.
[5] School of Ocean and Earth Science, National Oceanography Centre, University of Southampton, Southampton SO14 3ZH, UK.
[6] Alfred Wegener Institute, Am Handelshafen 12, 27570 Bremerhaven, Germany.
[7] Instituto de Investigaciones Marinas, CSIC, 36208 Vigo, Spain.

Corresponding author: Lidia I. Carracedo (lcarrace@ifremer.fr), https://orcid.org/0000-0003-3316-7651

Key Points:

- The overturning circulation lower limb drives a net southward transport of oxygen and nutrients from the North to the South Atlantic
- Anomalous circulation in 2010 enhanced nutrient convergence by the overturning upper limb, boosting North Atlantic biological CO_2 uptake
- We observed a deep silicate divergence in the North Atlantic in 2004 and 2010 compatible with a transient response to reduced overturning

Abstract

The North Atlantic Basin is a major sink for atmospheric carbon dioxide (CO_2) due in part to the extensive plankton blooms which form there supported by nutrients supplied by the three-dimensional ocean circulation. Hence, changes in ocean circulation and/or stratification may influence primary production and biological carbon export. In this study, we assess this possibility by evaluating inorganic nutrient budgets for 2004 and 2010 in the North Atlantic based on observations from the transatlantic A05-24.5°N and the Greenland-Portugal OVIDE hydrographic sections, to which we applied a box inverse model to solve the circulation and estimate the across-section nutrient transports. Full water column nutrient budgets were split into upper and lower meridional overturning circulation (MOC) limbs. According to our results, anomalous circulation in early 2010, linked to negative-NAO conditions, led to an enhanced northward advection of more nutrient-rich waters by the upper overturning limb, which resulted in a significant nitrate and phosphate convergence north of 24.5°N. Combined with heaving of the isopycnals, this 'extreme circulation event' in 2010 favoured an enhancement of the nutrient consumption (5.7 ± 4.1 kmol-P s^{-1}) and associated biological CO_2 uptake (0.25 ± 0.18 Pg-C yr^{-1}, upper-bound estimate), which represents a 50% of the mean annual sea–air CO_2 flux in the region. Our results also suggest a transient state of deep silicate divergence in both years. Both results are indicative of a MOC-driven modulation of the biological carbon uptake (by the upper MOC limb) and nutrient inventories (by the lower MOC limb) in the North Atlantic.

1 Introduction

Oceans play a crucial role in the climate system (Siedler et al., 2001). The capacity of the ocean to uptake and store atmospheric CO_2 emitted by human activities buffers the effects of the anthropogenically-induced perturbations on the global carbon cycle (Khatiwala et al., 2013; Heinze et al., 2015). This anthropogenic uptake by the solubility pump (2.6 Pg-C yr^{-1}; Gruber et al., 2019) is however small compared to the much larger natural carbon cycle including the roughly 10 Pg-C yr^{-1} exported from the upper ocean via the biological carbon pump (BCP) consisting of the production, sinking and remineralization of organic matter (Falkowski et al., 1998; Ito & Follows, 2005). Small

55 changes in natural carbon uptake therefore have the potential to negate or amplify
56 oceanic uptake of anthropogenic carbon. Such changes are likely because the BCP is
57 not homogeneously distributed across the ocean, particularly due to limitations imposed
58 by the lack of nutrients in the photic layer (upper 100-150 dbar) (Pérez et al., 2003;
59 Carpenter & Capone, 2013; Moore et al., 2013). The strongly stratified subtropical gyres
60 are some of the most extensive oligotrophic areas (Emerson et al., 2001), whereas the
61 high latitudes, especially the subpolar North Atlantic (Pommier et al., 2009), are
62 characterized by elevated winter nutrient concentrations which support extensive
63 phytoplankton blooms in spring (Watson et al., 2009).

64 Nutrients in the upper ocean are provided from multiple sources/mechanisms including
65 coastal runoff, atmospheric deposition, horizontal advection, isopycnal heave, wind-
66 driven upwelling, diapycnal diffusion and/or induction (e.g. Williams & Follows, 2003). The
67 importance of these mechanisms varies by region, with the Gulf Stream, so called
68 'nutrient stream' (Pelegrí & Csanady, 1991), being key in supplying nutrients from the
69 tropics to the mid and high latitudes in the Atlantic (Williams et al., 2011) and sustaining
70 primary production in the subtropical gyre via lateral advection (Palter et al., 2005, 2011;
71 Pelegrí et al., 2006; Dave et al., 2015; Letscher et al., 2016) and subsequent induction
72 downstream (Williams et al., 2006). The Gulf Stream forms the western boundary of the
73 subtropical gyre and comprises the bulk of the warm northward upper limb of the Atlantic
74 Meridional Overturning Circulation (MOC) (Meinen et al., 2010). Changes in ocean MOC
75 are closely linked with the North Atlantic Oscillation (NAO), the leading mode of
76 atmospheric variability in the North Atlantic, on interannual to decadal timescales
77 (Stepanov & Haines, 2014; DeVries et al., 2017; Sutton et al., 2017). The NAO evolved
78 from largely positive states in the 1990s to near neutral states in the 2000s (Hurrell et al.,
79 2013), reaching exceptionally negative values in 2010 (Osborn, 2011; Stendardo &
80 Gruber, 2012). The latter led to an anomalous southward Ekman transport and a
81 weakening of the MOC at 26.5°N (Srokosz & Bryden, 2015), with potential effects on the
82 nutrient supply to the upper ocean (Oschlies, 2001; Cianca et al., 2007).

83 Since nutrient availability limits primary production, any change in oceanic nutrient
84 content and supply to the photic layer has the potential to influence the regional
85 magnitude and/or efficiency of the BCP (Stocker et al., 2013). The assessment of basin-

scale nutrient pools and their variability is therefore crucial to our understanding of how the BCP functions and what factors control its magnitude and efficiency. Several studies have examined the large-scale meridional transport of major nutrients (nitrate, phosphate, and silicate) in the North Atlantic (Schlitzer, 1988; Rintoul & Wunsch, 1991; Martel & Wunsch, 1993; Williams & Follows, 1998; Williams et al., 2000; Álvarez et al., 2002, 2003, 2004; Ganachaud & Wunsch, 2002; Lavín et al., 2003; Williams et al., 2011; Maze et al., 2012), whereas fewer studies have provided nutrient budget estimates in the region (Michaels et al., 1996; Ganachaud & Wunsch, 2002; Álvarez et al., 2003; Maze et al., 2012; Fontela et al., 2019). Due to the differences and limitations of the methodological approaches, whether the North Atlantic is a net source for nutrients to the other basins remains subject to debate (Table 1). The inability to accurately assess time varying sources and sinks, as well as the scarcity of observational data that would allow estimation of accurate tracer accumulation/depletion rates at a basin scale, has traditionally resulted in a steady-state condition becoming a *de facto* assumption for the majority of the inverse nutrient budget calculations. The steady-state assumption implies the nutrient inputs and outputs are in balance so that the basin does not accumulate or lose nutrients in time. Only a very few studies indicated that the North Atlantic nutrient stocks might not be in steady state on decadal to century time-scales (e.g. Michaels et al., 1996). In this study we re-evaluate the nutrient budgets in the North Atlantic using the wealth of data collected since the last estimates by Álvarez et al. (2003). We consider the response of North Atlantic nutrient budgets to changing circulation and the likelihood that these budgets are not in steady state on annual-to-interannual timescales, suggesting that the biogeochemical budgets are subject to transient responses to the large (and rapid) MOC changes.

The study is structured as follows: in section 2 we present the data and methods; in section 3.1, we examine the basin-scale meridional nutrient (and oxygen) distributions and transports across both sections, accounting for the differences between both occupations (2004 and 2010); next, in section 3.2, by combining both hydrographic sections and recent estimates of external nutrient sources, we quantify the nutrient budgets of the region between the sections in both years to test the hypothesis that the

North Atlantic is in a biogeochemical steady state; and finally, section 4 contains the summary and conclusions.

Table 1. Summary of reference observation-based estimates of the meridional nutrient and oxygen transports at different latitudes in the North Atlantic. Negative transports meaning southwards.

Section	Cruise	Date		Property transport (kmol s^{-1})				Steady-state assumption	Reference
				Silicate	Nitrate	Phosphate	Oxygen		
Davis Strait (67ºN)	ARK-XXI 1b	16 Aug – 9 Sep	2005	-42.9 ± 5.2	-31.3 ± 3.6	-3.7 ± 0.4	np[a]	Yes	Torres-Valdés et al. (2013)
OVIDE (40-60ºN)	35TH20020610	10 Jun – 12 Jul	2002	np	11 ± 16	-0.2 ± 1	-924 ± 314	Yes	Maze et al. (2012)
	35TH20040604	4 Jun – 7 Jul	2004						
	06MM20060523	21 May – 28 Jun	2006						
	35TH20080610	10 Jun – 10 Jul	2008	-130 ± 50*	10 ± 35*	1.1 ± 3.6*	-2070 ± 600*	No	Fontela et al. (2019)
	35TH20100610	8 Jun – 7 Jul	2010						
	29AH20120622	23 Jun – 12 Aug	2012						
	35PK20140515	20 May – 26 Jun	2014						
	29AH20160617	17 Jun – 31 Jul	2016						
A25 (40-60ºN)	4x	7 Aug – 17 Sep	1997	-26 ± 15 np	-50 ± 19 -16 ± 36	-6 ± 2 np	-1992 ± 440 np	Yes	Alvarez et al. (2002) Maze et al. (2012)
A02 (47ºN)	29HE06_1-3	14 Jul – 15 Aug	1993	-130 ± 50	10 ± 35	1.1 ± 3.6	-1750 ± 500	Yes	Ganachaud & Wunsch (2002)
A03 (36ºN)	Leg 1, Atlantis II-109	11 Jun – 9 Jul	1981	-134 ± 38	119 ± 35	np	-2940 ± 180	Yes	Rintoul & Wunsch (1991)
A05 (24.5ºN)	Leg 3, Atlantis II-109	12 Aug – 4 Sep	1981	-152 ± 56	-8 ± 39	np	-2600 ± 120	Yes	Rintoul & Wunsch (1991)
	29HE06_1-3	14 Jul – 15 Aug	1992	-220 ± 80 -254 ± 176	-50 ± 50 -130 ± 95	-7.6 ± 3.6 -12.6 ± 6.3	-2070 ± 600 -2621 ± 705	Yes Argued	Ganachaud & Wunsch (2002) Lavín et al. (2003)
A06 (7.5ºN)	35A3CITHER1_2	5 Jan – 19 Feb	1993	-160 ± 110	-70 ± 120	-1.0 ± 7	-1430 ± 950	Yes	Ganachaud & Wunsch (2002)

*Average transport estimates also considering the 2002, 2004 and 2006 cruises. np, not provided.

2 Data and Methods

2.1 Hydrographic data

We used the cruise data from the GO-SHIP A05-24.5°N (www.nodc.noaa.gov/ocads/oceans/RepeatSections/clivar_a05.html) and OVIDE (www.nodc.noaa.gov/ocads/oceans/RepeatSections/clivar_ovide.html) sections (Figure 1). Both sections comprise high-quality measurements at high spatial resolution of standard tracers such as temperature, salinity, nitrate, silicate, phosphate, oxygen and carbonate system variables (pH, alkalinity, DIC), making them a valuable observational database for the study of the biogeochemical transports in the North Atlantic. First sampled in 1957, the A05-24.5°N section has been occupied nine times over the last few decades. In this study, we used the Apr-May 2004 (Brown et al., 2010) and Jan-Feb 2010 (Atkinson et al., 2012) repeats. Among the nine biennial repeats of the OVIDE section, which was first carried out in 2002, we used Jun-July 2004 (Lherminier et al., 2010) and June 2010 occupations (Mercier et al., 2015) (Table 2). We selected the 2004 and 2010

repeats as they were carried out within the same year at both the subtropical and subpolar locations. Both sections combined together enclose an oceanic region comprising a significant part of the North Atlantic (namely NA-box hereinafter, Figure 2).

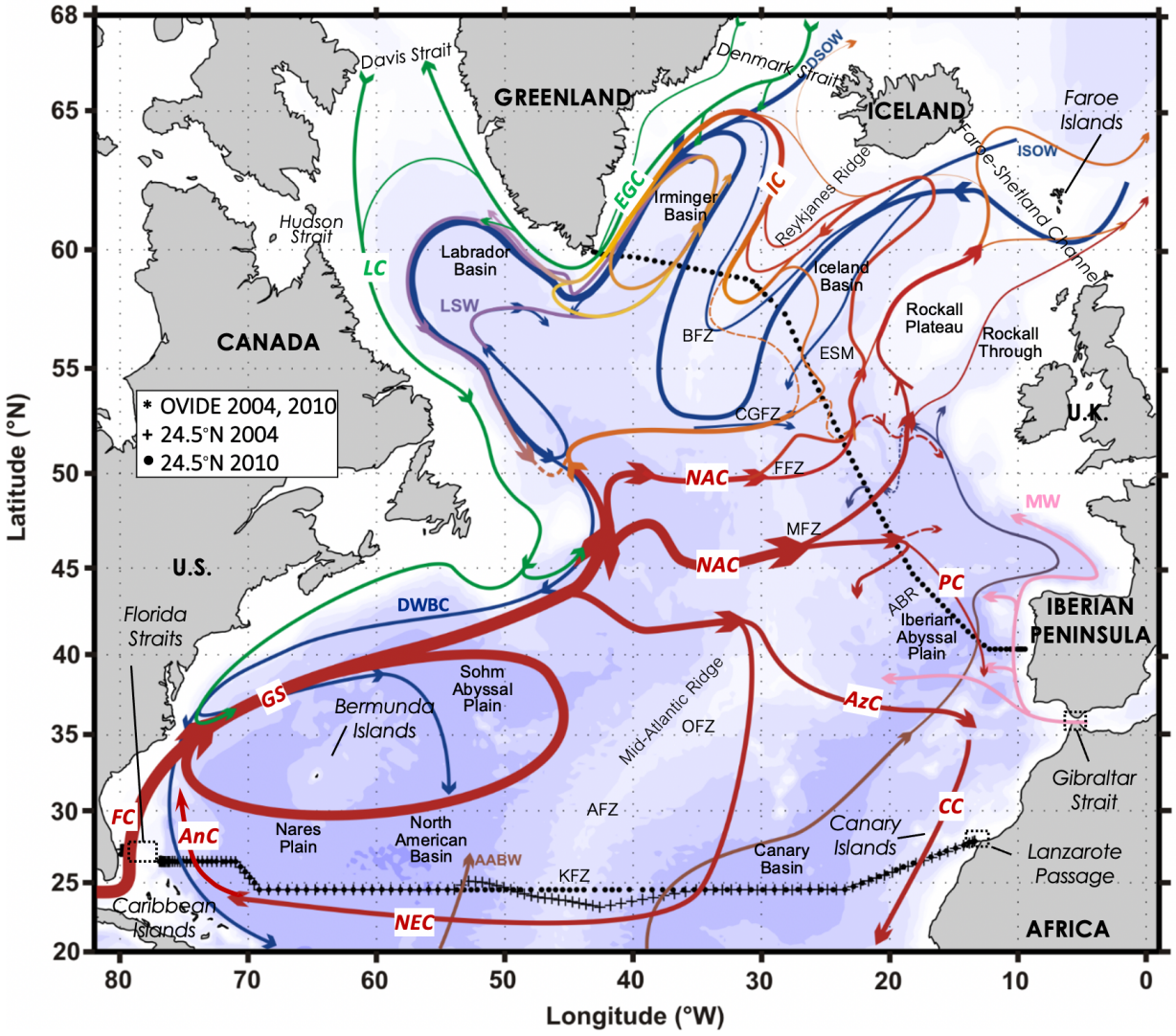

Figure 1. Schematic diagram of the North Atlantic circulation adapted from Daniault et al. (2016). Bathymetry is plotted with colour change at 100 m and every 1000 m at and below 1000 m. The locations of the A05-24.5°N and OVIDE hydrographic stations are indicated (see legend). The region enclosed by these two sections, and the Davis and Gibraltar Straits, is referred to as NA-box. Major topographic features: Azores-Biscay Rise (ABR), Atlantis Fracture Zone (AFZ), Bight Fracture Zone (BFZ), Charlie–Gibbs Fracture Zone (CGFZ), Eriador Seamount (ESM), Faraday Fracture Zone (FFZ), Kane Fracture Zone (KFZ), Maxwell Fracture Zone (MFZ), Oceanographer Fracture Zone (OFZ). Labelled

148 water masses and currents: Antarctic Bottom Water (AABW), Antilles Current (AnC),
149 Azores Current (AzC), Canary Current (CC), Deep Western Boundary Current (DWBC),
150 Denmark Strait Overflow Water (DSOW), East-Greenland Current (ECG), Florida Current
151 (FC), Gulf Stream (GS), Iceland–Scotland Overflow Water (ISOW), Irminger Current (IC),
152 Labrador Current (LC), Labrador Sea Water (LSW), Mediterranean Water (MW), North
153 Atlantic Current (NAC), North Equatorial Current (NEC), Portugal Current (PC).

154 **Table 2.** List of hydrographic cruises used in this study. C.S. denotes cruise chief
155 scientist, and #St the number of stations.

Section	Cruise Name	Expocode	Date		Vessel	C.S.	#St	Reference
OVIDE	OVIDE 2004	35TH20040604	4 Jun 7 Jul	2004	*Thalassa*	T. Huck	119	Lherminier et al. (2010)
	OVIDE 2010	35TH20100610	8 Jun 7 Jul	2010	*Thalassa*	V. Thierry	95	Mercier et al. (2015)
A05-24.5°N	CLIVAR A05 2004	74DI20040404	5 Apr 10 May	2004	*Discovery*	S. Cunningham	125	Atkinson et al. (2012)
	A05 2010	74DI20100106	6 Jan 15 Feb	2010	*Discovery*	B. King	135	

156 In the A05-24.5°N cruises, the analysis of inorganic nutrients, nitrate and nitrite
157 (hereinafter nitrate, NO_3^-), phosphate (PO_4^{3-}) and silicate ($Si(OH)_4$), were undertaken on
158 a Skalar San^{plus} autoanalyzer following the method described by Kirkwood (1996), with
159 the exception that pump rate through the phosphate line was increased by a factor of 1.5
160 to improve the reproducibility and peak shape of the results. OVIDE nutrients were
161 analysed using a Chemlab AAII type Auto-Analyser, following the protocols and methods
162 described by Aminot & Chaussepied (1983). The precision for NO_3^- and $PO_4^{3-}$and $Si(OH)_4$
163 was evaluated at 0.2, 0.02 and 0.1 µmol kg^{-1}, respectively. Oxygen was determined by
164 Winkler titration, following WOCE standards (Culberson, 1991) and GO-SHIP best
165 practices (Langdon, 2010) at OVIDE and A05-24.5°N, respectively, with a precision better
166 than 1 µmol kg^{-1}. All oxygen and nutrient data were quality controlled (QC) and corrected
167 according to GLODAPv2.2019 secondary QC protocols (Olsen et al., 2019) (see
168 multiplicative factors in Supporting Information Table S1).

169 2.2 Other data sources

170 In addition to cruise data, we used complementary hydrographic data (nitrate and neutral
171 density) from the Bermuda Atlantic Time-series Study (BATS) (http://bats.bios.edu/), and

MODIS satellite chlorophyll data (https://oceandata.sci.gsfc.nasa.gov/MODIS-Aqua/) for the period 2004 to 2012, to validate the anomaly signals detected in our data; the RAPID MOC time series data (Smeed et al., 2019), to compute the MOC magnitude for the period of the cruises and the annual averages, as a reference; and different wind product databases: the Cross-Calibrated Multi-Platform Product (CCMP) (Atlas et al., 2011), NCEP (Kistler et al., 2001) and ERA-Interim (Dee et al., 2011), to compute the Ekman transport across the sections.

Finally, to estimate the nutrient budgets in the NA-box (section 2.4), we also used additional data sources from former studies (Supporting Information Table S2) to account for the external inputs of nutrients by river runoff, atmospheric deposition, N_2-fixation, seafloor weathering, ground water, hydrothermal and meltwater sources, dissolved organic fraction or the nutrient transports across the open boundaries of the domain (Davis and Gibraltar Straits). Further details about derivation of numbers are provided in Supporting Information (Text S1).

2.3 Transports of nutrients

The transport of a tracer perpendicular to a transoceanic section (T_{tracer}; kmol s^{-1}) is estimated as

$$T_{tracer} = \sum_{j=stpA}^{stpB} \Delta x_j \int_{za}^{zb} \rho_j \, [tracer]_j \, v_j \, dz, \quad (1)$$

where T_{tracer} is the transport of the tracer (with *tracer* being the general notation for oxygen, O_2; silicate, $Si(OH)_4$; nitrate, NO_3; or phosphate, PO_4^{3-}) spatially integrated and positive (negative) into (out-of) the NA-box. For each station pair j, ρ_j is seawater density profile (kg m^{-3}), $[tracer]_j = [tracer](z)$ is the concentration of the tracer (in µmol kg^{-1}), and $v_j = v_j(z)$ is the (absolute) velocity profile (m s^{-1}). Δx is the horizontal coordinate (station pair spacing along the section, in m), with stpA and stpB referring to two different station pairs (note stpA=1 and stpB=N, with N the total number of stations pairs, when computing the net tracer transport across the entire section). Station pair notation refers to the mid-point between hydrographic stations, so that, e.g., stp1 refers to the midpoint between hydrographic stations 1 and 2. z is the vertical coordinate (either depth, in m, or density, in in kg m^{-3}), with za and zb referring to two different depths (note za=surface and

zb=bottom, when computing the net tracer transport across the entire section). To match the velocity fields, the oxygen and nutrient distributions were linearly interpolated at the same 1-dbar grid resolution as the velocity fields, and averaged across station pairs. For explanatory purposes, the transports of oxygen, nitrate, phosphate and silicate will be referred to hereinafter as kmol-O s^{-1}, kmol-N s^{-1}, kmol-P s^{-1}, and kmol-Si s^{-1}, respectively. Uncertainties for all nutrient transport estimates were estimated based on the uncertainty of each of the component parts of equation (1) (detailed in Supporting Information Text S2).

Absolute velocities across the A05-24.5°N and OVIDE sections ($v_j(z)$, Figure 2), were obtained by applying a box inverse model method (Mercier, 1986) founded on the least-squares formalism. The thermal wind equation is used to compute the relative geostrophic velocity, normal to the hydrographic section, which depends on the *a priori* selected reference layer. The objective of the inversion is to refine the velocity estimates at the reference level by minimizing—in the least squares sense—a set of constraints given by independent estimates (e.g. ADCP measurements and/or integral volume or tracer transports) and the distance to the *a priori* solution. For the A05-24.5°N – OVIDE joint inversion, we selected the reference levels, as well as a number of a priori constraints (Table 3), according to previous studies at the A05-24.5°N section (Lavín et al., 2003, and Atkinson et al., 2012) and the OVIDE section (Lherminier et al., 2007, 2010, and Mercier et al., 2015), while satisfying salt conservation (Supporting Information Text S3, Figures S1 and S2).

Table 3. Volume (Sv; 1 Sv=10^6 m^3 s^{-1}) and salt (Sv psu) transport constraints used in the 24.5°N – OVIDE joint inverse model. Positive transports mean into the NA-box, that is, southwards across the OVIDE section and northwards across the 24.5°N.

Constraints	Lon (°W)	Station pairs	Vertical range	Before inversion *a priori* value	After inversion value	References
OVIDE section						
2004						
Sal conservation	9.5-42.8	121-225	surf-bottom	-41.2 ± 35.0 Sv psu	-41.7	This study*
Vol conservation	9.5-42.8	121-225	surf-bottom	-1 ± 3 Sv	-0.9	Lherminier et al. (2010)
Eastern Boundary	9.5-10.7	121-128	surf-σ_2 36.98 kg m^{-3}	-5 ± 3 Sv	-3.1	Lherminier et al. (2010)
Eastern Boundary	9.5-10.7	121-128	σ_2 36.98 kg m^{-3}-bottom	-1 ± 2 Sv	-1.3	Lherminier et al. (2010)
IAP	11.1-16.4	129-145	σ_4 45.85 kg m^{-3}-bottom	-0.8 ± 0.8 Sv	-0.7	Lherminier et al. (2010)

2010						
Sal conservation	9.5-42.8	133-224	surf-bottom	-24.1 ± 35.0 Sv psu	-26.4	This study*
Vol conservation	9.5-42.8	133-224	surf-bottom	-1 ± 3 Sv	-0.4	Mercier et al. (2015)
IAP	9.5-22.5	133-174	σ_4 45.84 kg m^{-3}-bottom	-1.0 ± 1.0 Sv	-0.9	Mercier et al. (2015)
A05-24.5°N section						
2004						
Florida Current	77-80	1-8	0-800 dbar	31.8 ± 1.0 Sv	31.5	Baringer & Larsen (2001)
Atlantic Basin	13.4-77	9-120	surf-bottom	-36.4 ± 3.0 Sv	-37.1	Atkinson et al. (2012)
Sal conservation	13.4-80	1-120	surf-bottom	-26.0 ± 35.0 Sv psu	-23.4	McDonagh et al. (2015)
Vol conservation	13.4-80	1-120	surf-bottom	-1 ± 3 Sv	-1.0	This study*
2010						
Florida Current	77-80	1-11	0-800 dbar	30.5 ± 0.8 Sv	30.2	Baringer & Larsen (2001)
Atlantic Basin	13.4-77	12-132	surf-bottom	-33.5 ± 3.0 Sv	-34.0	Atkinson et al. (2012)
Sal conservation	13.4-80	1-132	surf-bottom	-26.0 ± 35.0 Sv psu	-21.1	McDonagh et al. (2015)
Vol conservation	13.4-80	1-132	surf-bottom	-1 ± 3 Sv	-0.8	This study*

* See Supporting Information Text S3 for derivation of numbers

The ageostrophic Ekman transport was estimated by means of the wind stress fields from the Cross-Calibrated Multi-Platform Product (CCMP) (Atlas et al., 2011), following McCarthy et al. (2012). A comparison between three different wind products, CCMP, NCEP (Kistler et al., 2001) and ERA-Interim (Dee et al., 2011) was done to validate our choice (Supporting Information Figure S1). The Ekman transport was averaged over the year of the cruise (annual average), and added homogeneously in the first 30 m of the water column. For both cruises and locations, seasonal aliasing did not exceed the range of the uncertainties associated with the annual estimates (Supporting Information Text S4). More details about methods and the sensitivity tests performed are provided in the Supporting Information (Texts S5 and S6).

The net volume transports across the study sections were geographically delimited by subregions (Figure 2). We selected the lateral limits of the regions so that they comprised main reference geographic limits and/or main current systems. Horizontally, we defined four main layers by isopycnal levels limiting the main water masses:

i) an upper-intermediate layer embracing the upper limb of the MOC, from surface to σ_1=32.15 kg m^{-3} (hereinafter referred to as σ_{MOC}; Mercier et al., 2015), which at 24.5°N is occupied by Central Waters (of North and South Atlantic origin) and Antarctic Intermediate Water (AAIW) (Guallart et al., 2015), and at OVIDE by North Atlantic Central Water (NACW), Subarctic Intermediate Water (SAIW) and Subpolar Mode Water (SPMW) (García-Ibáñez et al., 2015);

ii) an intermediate-deep layer, $\sigma_{MOC}<\sigma_1\leq32.53$ kg m^{-3} ($\sim\sigma_2=36.94$ kg m^{-3}), where at 24.5°N there is contribution of Mediterranean Water (MW), Labrador Sea Water (LSW), and upper North Atlantic Deep Water ($NADW_U$; of which the main source is the lightest vintage of the LSW) (Guallart et al., 2015), and at OVIDE contribution of SPMW, MW and LSW (García-Ibáñez et al., 2015);

iii) a deep layer, between $\sigma_1\leq32.53$ kg m^{-3} and $\sigma_4<45.9$ kg m^{-3}, which main contribution at 24.5°N is the lower North Atlantic Deep Water ($NADW_L$), and at OVIDE lower North East Atlantic Deep Water ($NEADW_L$), Denmark Strait Overflow Water (DSOW), and Iceland–Scotland Overflow Water (ISOW) (García-Ibáñez et al., 2015);

iv) and a bottom layer, $\sigma_4<45.9$ kg m^{-3}, only present at 24.5°N, mainly occupied by Antarctic Bottom Water (AABW) (Hernández-Guerra et al., 2014; Guallart, Schuster, et al., 2015).

σ_{MOC} was defined by Mercier et al. (2015) as the density at which the overturning stream function reaches a maximum across the OVIDE section. At this latitude, using density coordinates provides a more truthful magnitude of the overturning circulation (Lherminier et al., 2010), as it takes into account the fact that most of the East Greenland-Irminger Current (Figure 1) ultimately belongs to the lower limb of the MOC, while the North Atlantic Current (Figure 1) at the same depths belongs to the upper limb (Figure 2b,d). At 24.5°N, however, the overturning streamfunction is usually computed in depth coordinates, so that it represents a balance between net northward (southward) flowing water above (below) the depth of maximum overturning, located at around 1100 m (Smeed et al., 2014; McCarthy et al., 2015). The 1100 m level at this latitude is though pretty much concordant with the σ_1 = 32.15 kg m^{-3} isopycnal (Figure 2a,c). To be consistent at both locations, we kept the same upper/lower MOC limb interface definition as at the OVIDE section (i.e., $\sigma_{MOC}=\sigma_1=32.15$ kg m^{-3}). Transport-weighted properties by the upper and lower MOC limbs were estimated as the total tracer transport across the given MOC limb, divided by the volume transport by that limb.

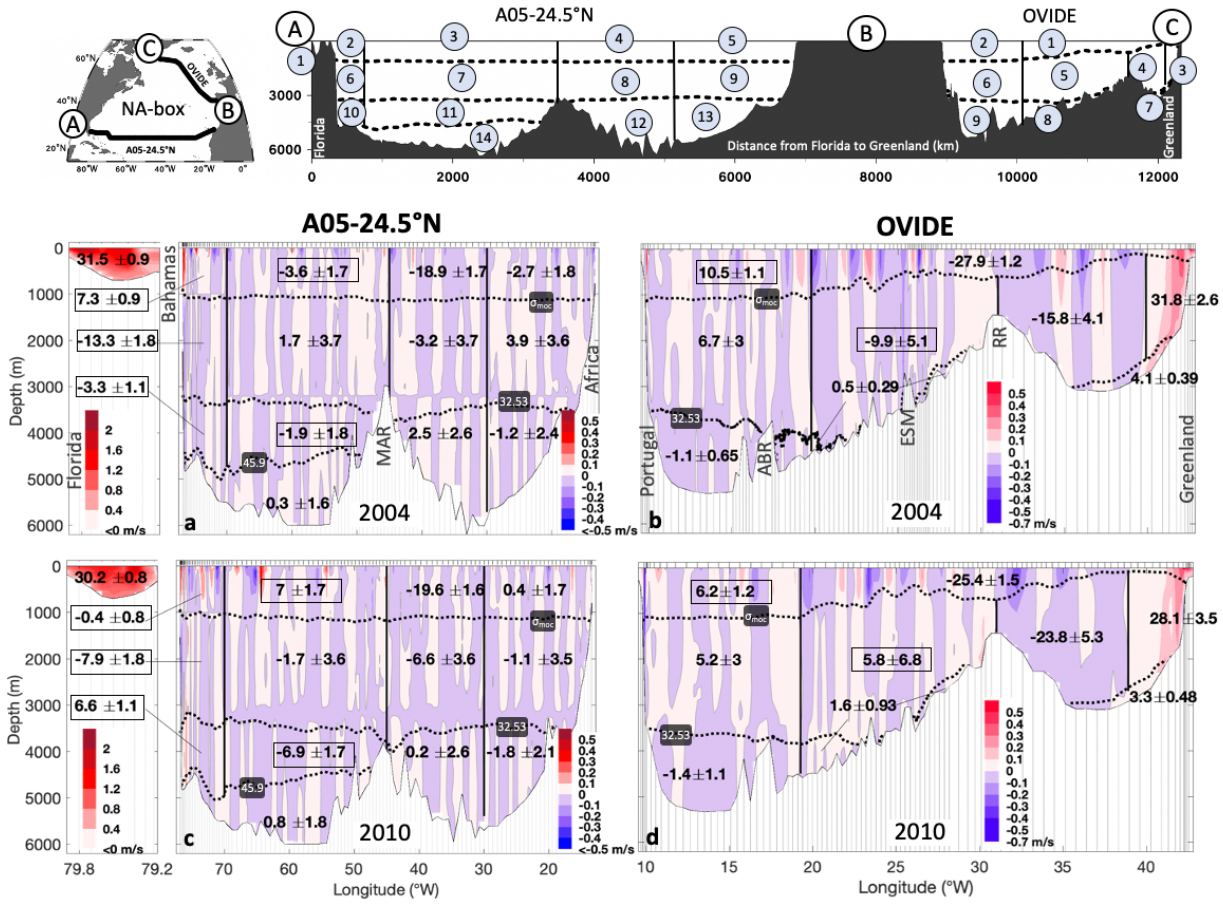

Figure 2. Upper panels: Schematic view of the NA-box (distances are to scale). Numbers in the open circles indicate subregion numeration, as reference for the results section. Lower panels: Velocity (in m/s) perpendicular to the A05-24.5°N (a,c) and OVIDE (b,d) sections for the 2004 (upper row) and 2010 (lower row) cruises. Panel b modified from Lherminier et al. (2010). The isopycnals used as density horizons for the nutrient transport estimates are also indicated (dotted lines): σ_{MOC} refers to σ_1 isopycnal 32.15 kg m^{-3} (σ_1 is the potential density referenced to 1000 dbar), separating the upper and lower limbs of the Atlantic Meridional Overturning Circulation (Mercier et al., 2015); σ_1=32.53 kg m^{-3} ; σ_4=45.9 kg m^{-3} (σ_4 is the potential density referenced to 4000 dbar). Numbers represent net transports ± uncertainties (in Sv, positive into NA-box) by subregions. Open squares indicate those regions where volume transports are significantly different for both years. Main topographic features are indicated: Azores-Biscay Rise (ABR), Eriador Seamount (ESM), Reykjanes Ridge (RR), Mid-Atlantic Ridge (MAR).

2.4 Budget estimates

As the main goal of the study, we estimated the silicate, nitrate and phosphate budgets in the NA-box. The NA-box was defined as the region bounded by the basin-scale subtropical A05-24.5°N section, the subpolar OVIDE section, and the Davis and Gibraltar Straits (Figure 1). The nutrient budgets, which satisfy the salt conservation (Supporting Information, Text S3), were defined as the balance between the following five main terms: lateral nutrient advection across the limits of NA-box (i.e., across the OVIDE section , T_N^{ovide}; the A05-24.5°N section, T_N^{a05}; the Davis Strait, T_N^{davis}; and the Gibraltar Straits, $T_N^{gibraltar}$), the nutrient supply by river runoff (F_N^{runoff}), the input through the air-sea interface within the enclosed domain ($F_N^{air-sea}$), the net biological nutrient source/sink term (B), and the time derivative of the nutrient content ($\frac{\Delta N}{\Delta t}$):

$$\frac{\Delta N}{\Delta t} = T_N^{ovide} + T_N^{a05} + T_N^{davis} + T_N^{gibraltar} + F_N^{runoff} + F_N^{air\text{-}sea} + B \quad (3)$$

Where subindex N refers to a general notation for nutrient (either silicate, $Si(OH)_4$; nitrate, NO_3; or phosphate, PO_4^{3-}). T_N^{ovide} and T_N^{a05} are the nutrient transports estimated according to equation (1) (section 2.3), whereas T_N^{davis}, $T_N^{gibraltar}$, F_N^{runoff} and $F_N^{air\text{-}sea}$ were obtained and/or inferred from previous studies (Supporting Information, Text S1 and Table S2). The term B accounts for the net balance between the organic matter production (nutrient sink) and remineralization (nutrient source), i.e., the net storage of organic matter (dissolved and particulate). Under a *de facto* steady-state assumption, the North Atlantic basin is not accumulating or losing nutrients ($\Delta N/\Delta t = 0$), so that the balance of inputs minus outputs must equal the biological term B within the box, which consequently becomes the target unknown in equation (3). More specifically, for the silicate budget, B accounts for the balance between biogenic silica production by silicifying plankton vs. biogenic silica dissolution (silicate regeneration); whereas for nitrate and phosphate, B refers to the balance between photosynthesis vs. respiration of organic matter (nitrate/phosphate regeneration). Most production is remineralized (either in surface or at depth), so in an integrated water column sense, B can only represent either: 1) sediment burial (which is a very small term compared to primary production and export production)

or 2) accumulation in a small particulate pool or larger dissolved organic pools. In the sense where water column is split (e.g. upper and lower limb, uMOC and lMOC, respectively), B^{uMOC} and B^{lMOC} represent net community production in the upper limb (if $B^{uMOC}>0$) and remineralisation in the lower limb (if $B^{uMOC}<0$). These indirect estimates B^{uMOC} and B^{lMOC} can be compared, under certain assumptions, with independent estimates of production and remineralization. Significant larger/lower values of B than those obtained by *in situ* measurements may be indicative of the existence of a time tendency in the nutrient budgets (i.e., $\Delta N/\Delta t \neq 0$), as will be discussed in section 3.2.

For silicate, we took into account the additional contribution of submarine groundwater, seafloor weathering, deep-sea hydrothermal sources (Tréguer & Rocha, 2013) and sheet-ice melting (Hawkings et al., 2017) as an extra addend in equation 3, $F_{silicate}^{other}$ (Supporting Information, Text S1.5 and Table S2). For nitrate, there is also an extra addend in equation (3), corresponding to the balance between biological dinitrogen fixation vs. denitrification ($F_{nitrate}^{N2\text{-}fixation}$) (Supporting Information, Text S1.4 and Table S2). Furthermore, when it comes to closing the nitrate and phosphate nutrient budgets in the North Atlantic, one agreed limitation among most of previous studies in the region (Michaels et al., 1996; Ganachaud & Wunsch, 2002; Álvarez et al., 2003; Fontela et al., 2019) is the contribution of the dissolved organic nutrient source from the subtropics to higher latitudes, suggested as the potential missing counter-balancing flux that might keep the inorganic nutrient pool in the North Atlantic in balance. We therefore also assessed the organic nutrient transport at 24.5°N (Supporting Information, Text S1.5 and Table S2).

In this study we present the nutrient budgets as net budgets (whole-water column integration), and split into upper (surface to σ_{MOC}) and lower (σ_{MOC} to bottom) MOC limb budgets.

3 Results and Discussion

3.1 Oxygen and nutrient distribution and transports across the A05-24.5°N and OVIDE sections

3.1.1 Oxygen and nutrient distributions: general description

The lowest nutrient concentrations are found in surface waters (Figure 3e to j) where they are consumed by phytoplankton activity, whereas oxygen concentrations in surface waters (Figure 3c,d) are relatively high due to direct exchange with the atmosphere (oxygen solubility). At intermediate levels, nutrients increase (oxygen decreases) due to *in situ* remineralization and ageing of the water masses (i.e., organic matter remineralization as water masses are laterally advected from their source regions). This biological process is responsible of the highest nitrate and phosphate concentrations at 24.5ºN being found at around 700-900 m (maximum remineralization depth) (Figure 3g,i), which is also evidenced by the pronounced oxygen minimum (namely oxygen minimum zone, Figure 3c). Deeper in the water column, high oxygen concentrations relate to the recently ventilated LSW (Figure 3c,d). Closer to the bottom, high nutrient concentrations (the highest for silicate, Figure 3e) are associated to the AABW, the oldest water mass across the section.

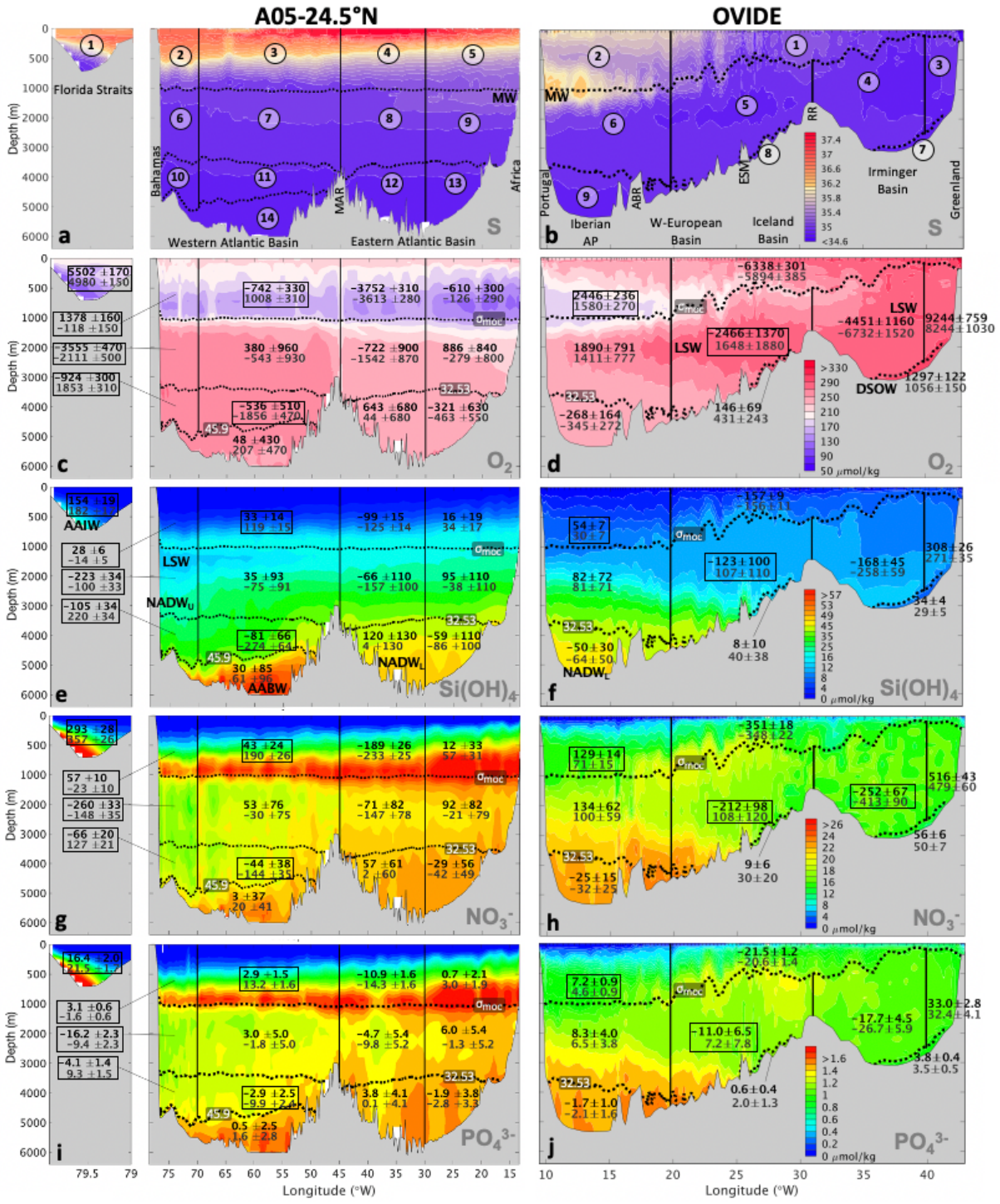

Figure 3. Vertical distribution of salinity (S), oxygen (O_2, in μmol kg^{-1}), silicate ($Si(OH)_4$, in μmol kg^{-1}), nitrate (NO_3^-, in μmol kg^{-1}) and phosphate (PO_4^{3-}, in μmol kg^{-1}) along the A05-24.5°N section (left panels) and the OVIDE section (right panels) for 2004. Numbers in the open circles in panels a and b indicate sub-region numeration, as reference for the

results section. Numbers in panels c to j represent oxygen and nutrient transports ± uncertainties (in kmol s^{-1}, positive into NA-box) by subregions. Open squares indicate those regions where oxygen and or nutrient transports are significantly different for both years. The isopycnals used in this study as density horizons for the nutrients transport estimates are also indicated (dotted lines): $\sigma_{MOC}=\sigma_1=32.15$ kg m^{-3} (σ_1 is the potential density referred to 1000 dbar); $\sigma_1=32.53$ kg m^{-3}; $\sigma_4=45.9$ kg m^{-3} (σ_4 is the potential density referred to 4000 dbar). Main water masses traceable by the oxygen and nutrient distributions are also indicated: Antarctic Bottom Water (AABW), Antarctic Intermediate Water (AAIW), Denmark Strait Overflow Water (DSOW), Labrador Sea Water (LSW), lower North Atlantic Deep Water ($NADW_L$), Mediterranean Water (MW), Subpolar Mode Water (SPMW), upper North Atlantic Deep Water ($NADW_U$); and main topographic features: Azores-Biscay Rise (ABR), Eriador Seamount (ESM), Reykjanes Ridge (RR), Mid-Atlantic Ridge (MAR).

3.1.2 Oxygen and nutrient mean circulation patterns

Here we describe the main circulation patterns at both locations. The transport values shown represent the average of the 2004 and 2010 occupations ± standard error (Table 4).

At 24.5ºN, the upper 1000 dbar (broadly upper MOC limb, $\sigma_1 \leq \sigma_{MOC}$, regions 1 to 5, Figure 3a) are characterized by a net northward transport of oxygen and nutrients as result of the large northward oxygen and nutrient transport by the Florida and Antilles Currents (regions 1+2, Figure 3a), which is not compensated by the gyre recirculation (regions 3+4+5). The lower MOC limb ($\sigma_1 > \sigma_{MOC}$, regions 6 to 14, Figure 3a), comprises a net southward transport of oxygen and nutrients, mainly advected by the Deep Western Boundary Current (DWBC) system (regions 6+7+10+11, Figure 3a). This current represents the largest transport of nutrients and oxygen across the whole section below 1000 dbar, although there is also a less intense deep southward transport of oxygen and nutrients in the eastern basin (regions 8+9+12+13, Figure 3a). Deeper in the water column, we find the bottom northward transport of oxygen and nutrients related to the AABW (region 14, Figure 3a). Dominated by the lower MOC limb, the net basin-wide (integration across the entire section) transport of oxygen and nutrients across 24.5ºN is

southwards (Table 4), consistent with previous estimates based on the 1992 A05 cruise (Jul-Aug) by Lavín et al. (2003) (-2621 ± 705 kmol-O s^{-1}, -254 ± 176 kmol-Si s^{-1}, -130 ± 95 kmol-N s^{-1} and -12.6 ± 6.3 kmol-P s^{-1}) and Ganachaud & Wunsch (2002) (-2070 ± 600 kmol-O s^{-1}, -220 ± 80 kmol-Si s^{-1}, -50 ± 50 kmol-N s^{-1} and -7.6 ± 3.6 kmol-P s^{-1}).

Across OVIDE, we identify the same upper/lower MOC scheme of circulation, with a net northward transport of oxygen and nutrients by the upper MOC limb ($\sigma_1 \leq \sigma_{MOC}$, regions 1 to 3, Figure 3b), which is mostly carried by the North Atlantic Current (region 1, Figure 3b) and partly recirculates in easternmost region of the section (region 2, Figure 3b); and a net southward transport of oxygen and nutrient by the lower MOC limb ($\sigma_1 > \sigma_{MOC}$, regions 3 to 9, Figure 3b). At this latitude, different to the A05-24.5°N results, the transport of nutrients by the upper and lower MOC limbs is nearly in balance, within the uncertainties (Table 4); although there is a significant net southward transport of oxygen. As part of the lower MOC, the Western Boundary Current (East Greenland-Irminger and Deep Western Boundary Currents, region 3, Figure 3b) is the main contributor to the basin-wide transports, comprising an intense southward "deep oxygen and nutrient stream", as observed at 24.5ºN. Below, the bottom southward transport related to the DSOW (region 7, Figure 3b) also contributes to the "deep oxygen and nutrients stream".

In the European Basin there is also a deep, albeit less intense, southward flux of oxygen and nutrients between 1000-4000 dbar pressure range (region 6, Figure 3b). Underneath, in the Iberian Abyssal plain, there is a net northward oxygen and nutrients transport (region 9, Figure 3b).

Integrated across the entire OVIDE section, only the transport of oxygen (2004: 1501 ± 770 kmol-O s^{-1}, 2010: 1398 ± 830 kmol-O s^{-1}, southward, Table 4) is significantly different from zero in both years (Table 3); a result consistent with estimates reported by Maze et al. (2012) (a three-cruise 2002-2006 mean: 924 ± 314 kmol-O s^{-1}) and Fontela et al. (2019) (an eight-cruise 2002-2016 mean: 909 ± 132 kmol-O s^{-1}). However, the enhanced MOC in 2010 produced nutrient transports that were large enough to be significant (81 ± 69 kmol-Si s^{-1}, -5.9 ±3.3 kmol-P s^{-1}). The only other significant non-zero net nutrient transport across OVIDE in the literature is the Fontela et al. (2019) eight-cruise average phosphate transport (-0.8 ± 0.7 kmol-P s^{-1}).

Between both sections, we estimated an across-σ_{MOC} upward diapycnal flux (1.8 ± 1.4 Sv in 2004, and 0.5 ± 1.6 Sv in 2010, Figure 6b,c) comprising an upward transfer of nutrients between the lower and upper MOC limbs. Although our result is below the uncertainty level, such diapycnal flow is supported by the study of Desbruyères et al. (2013), who found that about 4-Sv, related to the dense-to-light conversion of deep western boundary current waters, fed back into the upper MOC limb in the vicinity of Flemish Cap.

Table 4. Mean (2004 and 2010 average) volume, oxygen and nutrient transports (± standard error of the mean) by subregions and by lower/upper MOC limbs. Note that for the total section and upper and lower MOC limbs, transports by both years are also indicated. Region numbering is illustrated in Figures 2 and 3. Positive (negative) transports mean into (out of) the NA-box.

			Tvol (Sv)		**Toxy** (kmol s^{-1})		**Tsil** (kmol s^{-1})		**Tnit** (kmol s^{-1})		**Tphos** (kmol s^{-1})	
			2004	*2010*	*2004*	*2010*	*2004*	*2010*	*2004*	*2010*	*2004*	*2010*
			avg		*avg*		*avg*		*avg*		*avg*	
OVIDE		Total	-0.9 ± 3.7	-0.4 ± 3.6	1501 ± 310	1398 ± 350	-11 ± 28	81 ± 49	4 ± 16	45 ± 19	1.1 ± 1.1	6.7 ± 1.3
			-0.6 ± 0.2		1449.5 ± 51.9		35 ± 46		25 ± 20		3.9 ± 2.8	
		uMOC ($\sigma_1 \leq 32.15$)	-17.3 ± 0.9	-19.2 ± 1.3	-3892 ± 221	-4315 ± 324	-103 ± 6	-126 ± 9	-222 ± 12	-277 ± 18	-14.3 ± 0.9	-16 ± 1.1
			-18.3 ± 1		-4103 ± 211		-115 ± 12		-250 ± 0		-15.2 ± 0.9	
		lMOC ($\sigma_1 > 32.15$)	16.6 ± 1.2	18.8 ± 1.5	5393 ± 409	5712 ± 517	92 ± 27	208 ± 49	227 ± 18	322 ± 25	15.4 ± 1.1	22.8 ± 1.7
			17.7 ± 1.1		5553 ± 160		150 ± 58		274 ± 48		19.1 ± 3.7	
Upper	reg. 1	North Atlantic Current	-26.6 ± 1.3		-6116 ± 222		-156 ± 0		-350 ± 1		-21 ± 0.4	
	reg. 2	Eastern recirculation	8.4 ± 2.1		2013 ± 433		42 ± 12		100 ± 29		5.9 ± 1.3	
Intermediate	reg. 3	Western Boundary Current	30 ± 1.8		8744 ± 500		290 ± 18		498 ± 19		32.7 ± 0.3	
	reg. 4	Irminger Basin	-19.8 ± 4		-5591 ± 1141		-213 ± 45		-332 ± 80		32.7 ± 0.3	
	reg. 5	Iceland Basin	-2 ± 7.8		-409 ± 2057		-8 ± 115		-52 ± 160		-1.9 ± 9.1	
	reg. 6	European Basin	6 ± 0.8		1651 ± 240		82 ± 0		117 ± 17		7.4 ± 0.9	
Deep	reg. 7	Irminger Basin	3.7 ± 0.4		1177 ± 433		32 ± 2		53 ± 3		3.6 ± 0.2	
	reg. 8	East Reykjanes Ridge	1 ± 0.5		289 ± 142		24 ± 16		19 ± 10		1.3 ± 0.7	
	reg. 9	European Basin	-1.2 ± 0.1		-307 ± 38		-57 ± 7		-28 ± 3		-1.9 ± 0.2	
A05-24.5°N		Total	-0.98 ± 0.9	-0.8 ± 0.9	-2326 ± 310	-2558 ± 310	-122 ± 68	-250 ± 66	-50 ± 40	-33 ± 36	-4.2 ± 2.7	-2.2 ± 2.3
			-0.9 ± 0.1		-2442 ± 116		-186 ± 64		-42 ± 9		-3.2 ± 1.0	
		uMOC ($\sigma_1 \leq 32.15$)	13.7 ± 0.5	17.5 ± 0.4	1775 ± 88	2132 ± 71	132 ± 4	196 ± 4	215 ± 7	349 ± 6	12.3 ± 0.5	21.8 ± 0.4
			15.6 ± 1.9		1953 ± 178		164 ± 32		282 ± 67		17.1 ± 4.8	
		lMOC ($\sigma_1 > 32.15$)	-14.7 ± 1.7	-18.3 ± 1.4	-4101 ± 426	-4690 ± 362	-254 ± 55	-446 ± 48	-265 ± 35	-382 ± 31	-16.5 ± 2.5	-24 ± 2.1
			-16.5 ± 1.8		-4395 ± 294		-350 ± 96		-323 ± 58		-20.2 ± 3.8	
Upper	reg. 1+2+3	Florida Straits, W-Atlantic	36.0 ± 0.8		6004 ± 134		251 ± 36		458 ± 66		27.8 ± 5.3	
	reg. 4+5	E-Atlantic	-20.4 ± 1.2		-4051 ± 312		-87 ± 4		-176 ± 1		-10.7 ± 0.6	
D/I	6+7+10+11	DWBC system	-13.3 ± 3.5		-3646 ± 988		-301 ± 72		-255 ± 62		-16 ± 4.2	
	8+9+12+13	E-Atlantic	-3.7 ± 5.6		-877 ± 1362		-94 ± 184		-80 ± 128		-5.3 ± 8.5	
B	reg. 14	W-Atlantic	0.5 ± 0.3		128 ± 79		45 ± 15		12 ± 8		1.1 ± 0.5	

434 *3.1.3 2004-to-2010 differences in nutrient distributions and transports: upper vs lower*
435 *MOC limb-mediated meridional transport of oxygen and nutrients*

436 In this section, we first identify the major differences observed in the oxygen and nutrient
437 distributions and transports in 2010 compared to 2004 at both locations. Temporal
438 variations in oxygen and nutrient distributions may be caused by changes in circulation
439 patterns, i.e., more or less of a certain water mass crossing the section, and/or by
440 changes in the tracer concentrations within water masses. The latter in turn can be the
441 result of changing water mass properties in the source region, changes in the mixing with
442 surrounding waters as the water mass spreads, and/or due to variations in the biological
443 activity. Here, the comparison between both occupations seeks to better understand the
444 representativeness of our estimates with regards to a mean state, as well as the origin of
445 the differences observed, rather than aiming to infer changes over time *per se*.

446 At 24.5ºN, the most striking change was found at the nitrate and phosphate (oxygen)
447 maximum (minimum) depth (Figure 3c,g,i), around 700-900 dbar mainly in the Florida
448 Straits and western Atlantic, where the nutrient (oxygen) maximum (minimum) was
449 notably larger (lower) in 2010 compared to 2004 (Figure 4e,i,k). This large nutrient
450 increase at the thermocline level ranged between 4-7 μmol-N kg^{-1} and 0.2-0.4 μmol-P kg^{-1}
451 in the Florida Straits and Western Atlantic basin, with a section average increase at that
452 level of ~1 μmol-N kg^{-1} and ~0.05 μmol-P kg^{-1} (accompanied by a concomitant decrease
453 in oxygen of around 10 μmol kg^{-1}, Figure 4i). Several studies (e.g. García et al., 1998,
454 2005; Bopp et al., 2002; Matear & Hirst, 2003; Stramma et al., 2010; Stendardo & Gruber,
455 2012) have reported deoxygenation trends and expansion of hypoxic/suboxic waters at
456 the minimum oxygen zone (broadly 700-1000 m depth). Yet, the magnitude of these
457 trends (0.6 μmol-O_2 $kg^{-1}y^{-1}$ at 1100 m for the period 1957-1992 by García et al., 1998; or
458 0.09-0.34 μmol-O_2 $kg^{-1}y^{-1}$ in the 300-700 m by Stramma et al., 2008) do not account for
459 the 6-year change observed here, evidencing that further driving mechanisms in 2010
460 might have enhanced the long-term signal. The positive (negative) anomaly signature in
461 nutrients (oxygen) was also accompanied by negative anomalies in temperature (Figure
462 4c) and salinity (not shown), linked to positive density anomalies (Figure 5a), which can
463 be interpreted as isopycnal vertical displacement (heave).

Evidencing the relevance of these nutrient anomalies, we found that even though the Florida and Antilles Currents were significantly weaker in 2010 (29.8 ±1.1 Sv; regions 1+2, Figure 2c) compared to 2004 (38.8 ±1.3 Sv ; regions 1+2, Figure 2a), the nitrate and phosphate transports were not reduced accordingly in proportion (Figure 3g,i). That is, the nutrient transport in these regions in 2010 was not dominated by changes in volume transports but compensated instead by changes in nutrient concentration. Overall, both isopycnal heave and the enhancement of the northward transport in the entire upper western basin (regions 2 and 3, Figure 2a,c) led to more nutrient-rich and less oxygenated thermocline waters being advected across the section by the upper MOC in 2010 (Table 4). Combined with the gyre recirculation in the eastern basin not being significantly different in both years (reduced recirculation in 2010, but not statistically different of 2004 within the uncertainties), this resulted in a significant larger northward nutrient transport in the upper MOC compared to 2004 (Table 4).

In the lower MOC limb, we observed negative silicate anomalies (Figure 4g), especially in the eastern basin. These anomalies were linked to a northward-to-southward flow reversal in 2010 in regions 7 and 9 and enhanced southward flow in region 8 Figure 2a,c), which reduced the influence of southern-origin (silicate-rich) waters in the 1000-3500-dbar pressure range compared to 2004. In contrast to this enhanced southward volume transport by the lower MOC in the eastern basin, we found the DWBC system (regions 6+7+10+11, Figure 2) experienced a reduction in 2010 (-9.9 ±4.5 Sv, Figure 2c) compared to 2004 (-16.8 ±4.6 Sv, Figure 2a), which was statistically significant in its westernmost branch (regions 6+10, Figure 2). This decrease, consistent with the MOC slowdown recorded by the RAPID array (Smeed et al., 2018), led to a concomitant significant reduction of the southward nutrient transports by the DWBC (Figure 3e,g,i). West of the Mid-Atlantic Ridge below 3500 dbar, we also observed positive silicate anomalies (Figure 4g) linked to a larger influence of southern-origin waters in 2010 in this part of the section as result of the reduced DWBC transport (less northern-origin $NADW_L$ influence) (Figure 2a,c, regions 10, 11 and 12). Integrated across the section and from surface to bottom, the anomalous circulation pattern in 2010 resulted into total nitrate and phosphate transports that were not statistically different from zero (Table 4). Compared to the 2004 transports, a reduction of the meridional nitrate and phosphate total transport

of 34% and 48% respectively was thus observed. Total oxygen and silicate transports were larger in 2010 compared to 2004, although these temporal differences were within the range of the uncertainties.

At OVIDE, the North Atlantic Current (region 1) was weaker in 2010 (Figure 2b,d), consistent with the reduction of the Florida and Antilles Currents at 24.5ºN. Its southwards recirculation in the eastern basin (region 2) was also reduced in 2010, although this slowdown was more pronounced than the reduction in the North Atlantic Current, leading to the net oxygen and nutrient transports by the upper MOC limb to be significantly larger in 2010 compared to 2004 (Table 4). We identified a positive nitrate anomaly (of 5-7 μmol kg^{-1}, Figure 4j) over the Reykjanes Ridge that was not accompanied by a concomitant increase in phosphate. This positive anomaly patch was coincident with an intensification of the Irminger Current (Figure 2, b,d). The fact that the nitrate anomaly was not accompanied by a concomitant increase in phosphate, prompted us to hypothesize that the waters advected by the enhanced Irminger Current comprised an increased contribution of subtropical-origin waters, which are characterized by high N_2-fixation-derived nitrate concentrations relative to phosphate, as characterised by a positive N* (N-16P) anomaly (Gruber & Sarmiento, 1997; Benavides et al., 2013; Benavides & Voss, 2015). These results may comprise observational evidence of how under a negative-NAO scenario, the cyclonic circulation in the Newfoundland Basin strengthens so that the Labrador Current and its retroflection intensify (Henson et al., 2013; Sarafanov et al., 2009). We conjecture that the mixing between the Labrador Current and the NAC waters nearby Flemish Cap (Fratantoni & McCartney, 2010) might have been enhanced in 2010 and caused the observed downstream nitrate anomaly. The unusually large phytoplankton abundances in the central Irminger basin in 2010 were also suggestive of such intensified recirculation (Henson et al., 2013).

In the lower MOC limb, we observed positive nitrate and phosphate anomalies in the Irminger Basin (related to the explanation above), but negative anomalies east of the Reykjanes Ridge up to the Azores-Biscay Rise. The latter related to a to northward-to-southward flow reversal in the Iceland Basin in 2010 (region 5, Figure 2b,d), which led to

524 the advection of more recently-ventilated (with lower age) waters across the section in
525 2010.

526 The southward intensification of these 'secondary' southward deep flows in the eastern
527 basin across both the OVIDE and A05-24.5ºN sections counteracted the decrease in the
528 DWBC (Figure 2), hence not resulting in a noticeable annual MOC slowdown, as
529 estimated by the RAPID-array time series (12.8 Sv, Apr 2009-Mar 2010 average,
530 McCarthy et al., 2012; Bryden et al., 2014, Smeed et al. 2018; 15.0 [5.1] Sv, Jan-Dec
531 2010 average [standard deviation]; Smeed et al. 2019), but leading instead to a larger
532 MOC in 2010 than in 2004 (Table 4). In view of that, hereinafter we will refer to a DWBC
533 slowdown in 2010 rather than MOC slowdown.

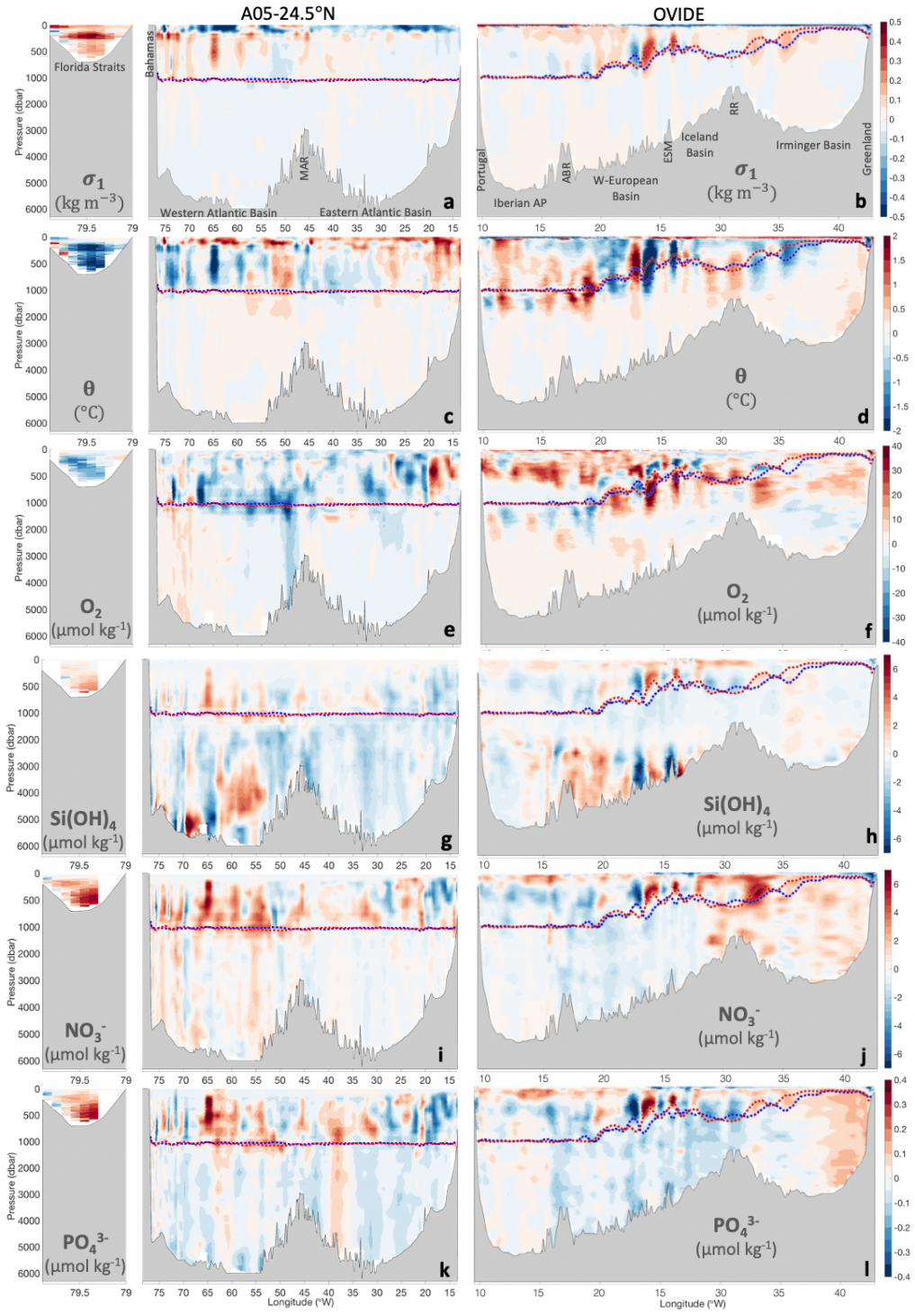

Figure 4. Vertical distributions of potential density (σ_1, potential density referred to 1000 dbar), potential temperature (θ), oxygen (O_2), silicate ($Si(OH)_4$), nitrate (NO_3^-) and phosphate (PO_4^{3-}) anomalies (2010 minus 2004) on pressure surfaces along the A05-

539 24.5°N section (left panels) and OVIDE section (right panels). Dotted lines correspond to
540 the σ_{MOC} isopycnal (2004 in blue, 2010 in red).

541 To better disentangle the overall change in properties between both sections and years,
542 we estimated the transport-weighted concentrations for the upper and lower branches of
543 the MOC (Table 5). Both MOC limbs are characterized by a meridional North-to-South
544 gradient of decreasing (increasing) oxygen (nutrient) concentrations (Figure 3, Table 5).
545 Biotic remineralization of the exported dissolved organic carbon at high latitudes (Fontela
546 et al., 2016), as well as dilution with the northward-flowing low dissolved organic carbon
547 Antarctic Intermediate and Bottom Waters (Hansell et al., 2009), support the observed
548 gradient. Oxygen is furthermore influenced by enhanced solubility of colder subpolar
549 waters (Gruber et al., 2001) and deep convection of recently ventilated waters, which
550 ultimately favours the transfer of this high-oxygen signal to depth (Fröb et al., 2016).
551 However, the lower MOC limb is more meridionally homogeneous for oxygen than the
552 upper limb, but with the largest silicate gradient. For nitrate and phosphate, the transport-
553 weighted properties suggest a more meridionally-homogeneous upper MOC in 2004, but
554 a more meridionally-homogeneous lower limb in 2010. Both the upper and lower MOC
555 limbs were enriched in nutrients in 2010 compared to 2004 at both sections. Note,
556 however, that at OVIDE the nutrient increase in the upper limb was only significant for
557 nitrate, whereas at A05-24.5°N the nutrient increase in the lower limb was only significant
558 for silicate. The latter would be explained by the reduced intensity of the DWBC, which
559 favoured the penetration of AABW northwards (Figure 2), and led to an overall significant
560 increase in the transport-weighted silicate concentration by the lower MOC limb (Table
561 5).

562 **Table 5.** Transport-weighted properties (oxygen, silicate, nitrate, phosphate) by upper
563 and lower MOC limbs (uMOC, lMOC).

		Transport (Sv)		Transport-weighted properties (µmol kg^{-1})							
				Oxygen		Silicate		Nitrate		Phosphate	
		2004	2010	2004	2010	2004	2010	2004	2010	2004	2010
uMOC	OVIDE	-17.3 ± 0.9^{g}	-19.2 ± 1.3	218 ± 16^{g}	220 ± 22^{g}	5.7 ± 0.4^{g}	6.4 ± 0.6^{g}	12.4 ± 0.9^{g,t}	14.1 ± 1.3^{g,t}	0.8 ± 0.1	0.8 ± 0.1^{g}
	A05	13.7 ± 1.0^{g,t}	17.5 ± 0.9^{t}	126 ± 16^{g}	119 ± 11^{g}	9.4 ± 1.6^{g,t}	11.0 ± 1.2^{g,t}	15.3 ± 2.6^{g,t}	19.4 ± 1.9^{g,t}	0.9 ± 0.2^{t}	1.2 ± 0.1^{g,t}
lMOC	OVIDE	16.6 ± 1.2	18.8 ± 1.5	320 ± 33	295 ± 35^{g}	5.5 ± 1.7^{g,t}	10.8 ± 2.7^{g,t}	13.4 ± 1.4^{g,t}	16.6 ± 1.8^{g,t}	0.9 ± 0.1^{t}	1.2 ± 0.1^{t}
	A05	-14.7 ± 1.2^{t}	-18.3 ± 1.1^{t}	273 ± 34	249 ± 24^{g}	16.9 ± 4.8^{g,t}	23.7 ± 3.7^{g,t}	17.6 ± 2.4^{g}	20.3 ± 1.8^{g}	1.1 ± 0.2	1.3 ± 0.1

564 ^{g} Superscript indicates a larger-than-uncertainty latitudinal property gradient; ^{t} Superscript indicates larger-than-
565 uncertainty temporal differences.

Overall, and even if hydrographic cruise data at 24.5ºN (17.5 ± 0.9 Sv, this study; 16.1 Sv, Atkinson et al., 2012) do not replicate the magnitude of the MOC slowdown in 2010 as reported by the RAPID array on an annual basis (15.0 [5.1] Sv average [standard deviation] for the 2010 Jan-Dec annual period; Smeed et al., 2019), even if considering the quasi-synoptic wind forcing to run the inversion (13.2 ± 0.9 Sv, this study, Supplementary Information Text S6; versus the RAPID-array estimate of 8.4 [1.7] Sv, average [standard deviation] for the period of the cruise; Smeed et al., 2019), the estimates are not inconsistent, since they represent different time scales and are based in different methodological approaches. In this study we did identify an anomalous pattern of advection in 2010 including anomalously negative Ekman transport, isopycnal heave, reorganization in the gyre circulation (McCarthy et al., 2012), weakening of the DWBC and strengthening at depth of the secondary southward advective branches, all of these physical drivers favouring the northward transport of more nutrient-richer waters by the upper MOC limb in 2010 (Table 3, Figure 5), which ultimately led to a reduced southward transport of nitrate and phosphate.

Ultimately, the results above may comprise observational evidence of how under a negative-NAO scenario, and favoured by the NAO-induced contraction of the Subpolar Gyre (Chaudhuri et al., 2011; Sarafanov et al., 2009), the contribution of subtropical and southern waters at high latitudes of the North Atlantic was enhanced, and compensating altered circulation patterns at depth observed.

3.2. Nutrient budgets in the North Atlantic

3.2.1 2004 vs. 2010 nutrient budgets in the North Atlantic

As an ultimate objective of this study, we provided novel estimates of the major inorganic nutrient inventories (silicate, nitrate and phosphate) in the North Atlantic, which had not been re-evaluated for this region since the former studies of Álvarez et al. (2003) and Ganachaud & Wunsch (2002). For the first time in this region, we combined two basin-scale hydrographic sections (the subtropical A05-24.5°N section and the subpolar OVIDE section) occupied in the same year for two different occupation periods (2004 and 2010), to derive consistent circulations across the sections using a joint inverse model and

595 compute the nutrient transports across them. Combining these basin-wide advective
596 nutrient transports with the most recent estimates of the additional external nutrient
597 sources (e.g. atmospheric inputs and river runoff) (Supporting Information, Table S2), we
598 obtained the net nutrient balance term (term B in equation (3)) for the North Atlantic, which
599 under steady-state ($\Delta N/\Delta t = 0$) leads to an inferred net biological nutrient source/sink in
600 the NA-box (Figure 5).

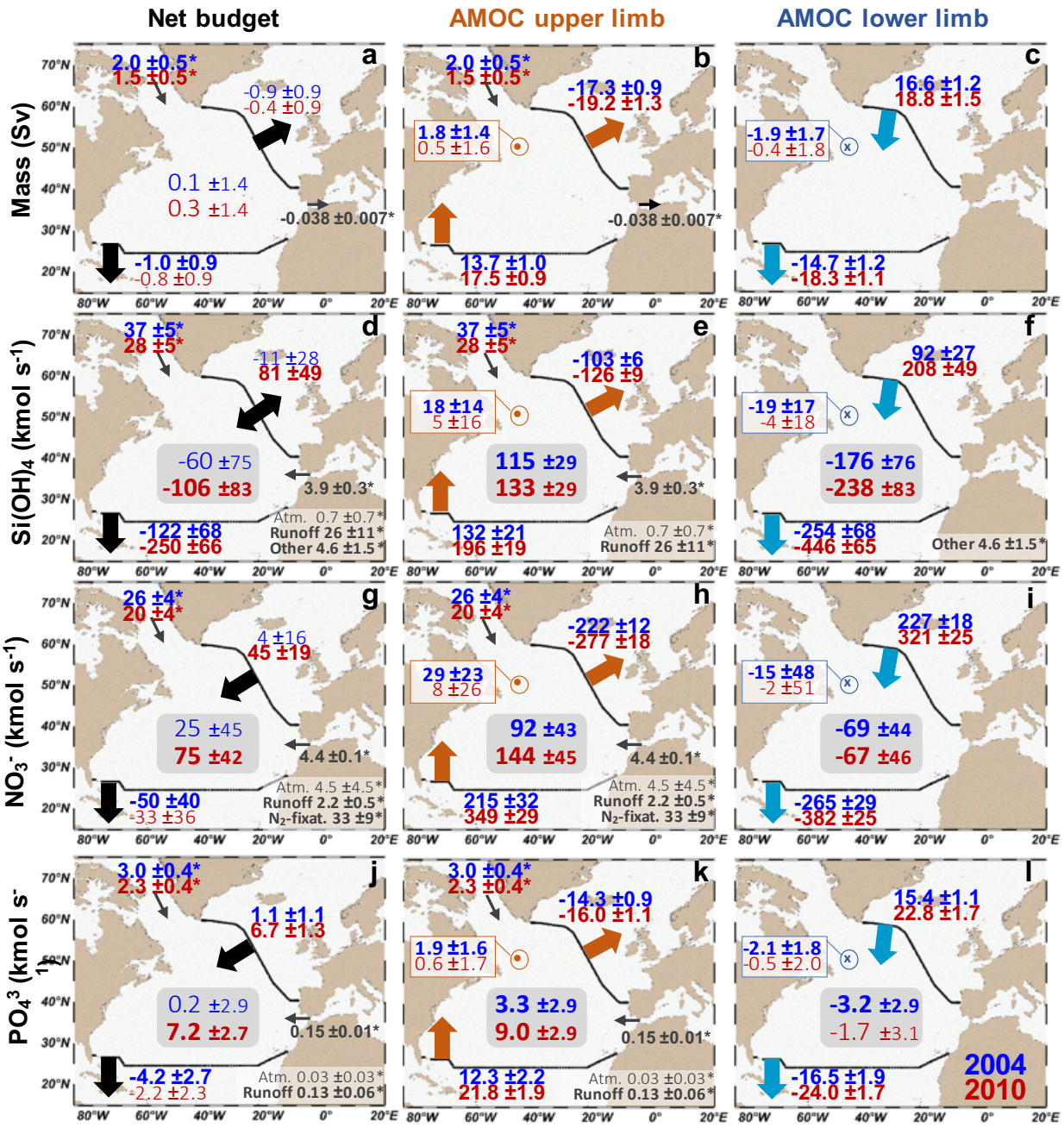

Figure 5. Schematic of the volume (a to c), silicate (d to f), nitrate (g to i) and phosphate (j to l) budgets in the North Atlantic. Left panels represent the net surface-to-bottom budgets, whereas the middle and left panels account for the upper and lower MOC limb budgets, respectively. Volume budget: large-font numbers account for the convergence/divergence term closing the budget (positive meaning net evaporation); for the upper (lower) MOC budgets, values outlined in orange refer to diapycnal flow, positive (negative) sign meaning inflow (outflow). Units in Sv (1Sv=10^6 m^3 s^{-1}). Inorganic nutrient

609 budgets: large-font numbers in the grey-shaded squares account for the net balance term
610 B in equation (3) (B for the net water-column integrated budget, left side panels; B^{uMOC}
611 for the upper MOC limb budget, central panels; or B^{lMOC} for the lower MOC limb budget,
612 right panels), positive values meaning nutrient convergence (net nutrient consumption
613 under steady-state); negative values meaning nutrient divergence (net nutrient
614 remineralization under steady-state). Units in kmol s^{-1}. Blue (red) numbers refer to 2004
615 (2010) budgets. Bold font indicates significantly different from zero values. Numbers with
616 an asterisk are referenced in the Supporting Information (Table S2).

617 Integrated over the whole water column, the net nutrient balance (term B in equation 3)
618 was statistically different from zero only in 2010 (B[2010]: -106 ± 83 kmol-Si s^{-1}, 75 ± 42
619 kmol-N s^{-1}, 7.2 ± 2.7 kmol-P s^{-1}, Figure 5d, g, j). In 2004, however, the system was close
620 to balance, with none of the net nutrient balance estimates B being significantly different
621 from zero (B[2004]: -60 ± 75 kmol-Si s^{-1}, 25 ± 45 kmol-N s^{-1}, 0.2 ± 2.9 kmol-P s^{-1}). Results
622 from the sensitivity analysis we performed (Supporting Information, Text S6) showed that
623 these net balance estimates are significantly sensitive to the wind forcing used to solve
624 the velocity field at 24.5°N in 2010 (annual *vs* synoptic forcing), with quasi-synoptic wind
625 forcing leading to significantly enhanced nutrient convergence (Supporting Information,
626 Figure S8), hence intensifying the anomalous pattern in 2010. Our annual estimates for
627 2010 might therefore represent a lower bound of the convergence occurred. However, for
628 nutrient budget estimate purposes, the annual forcing provides a more representative
629 approach of the real state as it prevents aliasing of seasonal imbalances, especially when
630 combining cruises that have been carried out in different seasons (Supporting
631 Information, Text S4); since we would be adding extra uncertainty due to the seasonal
632 imbalance linked to the biological term (balance term B in equation 3).

633 For nitrate and phosphate, the net balance term was positive, and statistically significant
634 in 2010, showing that under the steady state assumption, there is a significant net nutrient
635 consumption (75 ± 42 kmol-N s^{-1}, 7.2 ± 2.7kmol-P s^{-1}), which suggests the region acts as
636 a net autotrophically with biological primary production exceeding respiration (i.e., the
637 basin producing more organic carbon than that being consumed through
638 remineralisation). Relaxing the steady state assumption, nevertheless, another plausible

639 explanation could be that the region accumulated nitrate and phosphate during the period
640 ($\frac{\Delta N}{\Delta t}$>0, in equation 3). This result contrasts with a former study by Álvarez et al. (2003),
641 whose estimates pointed to a total nitrate production in the North Atlantic region. Their
642 estimate, the result of the sum of a net nitrate consumption between their 4x (OVIDE-like)
643 section and 36°N, and a net nitrate remineralization between 36°N AND 24.5°N, was
644 however not significantly different from zero (15 ± 131 kmol s^{-1}), which makes it
645 statistically comparable to our result in 2004.

646 Contrarily to nitrate and phosphate, the water-column integrated silicate budget resulted
647 in a negative balance term. For both years, the net silicate balance (B[2004]: -60 ± 75
648 kmol-Si s^{-1}; B[2010]: -106 ± 83 kmol-Si s^{-1}; its magnitude being only statistically significant
649 in 2010) indicated net silicate regeneration within the NA-box (i.e., net loss of biogenic
650 silica, under the steady-state assumption). Or, relaxing the steady state assumption, it
651 might be indicative of the North Atlantic losing silicate during the period ($\frac{\Delta N}{\Delta t}$ <0, in
652 equation 3).

653 The opposing sign in the water-column integrated net silicate balance vs that of nitrate
654 and phosphate, indicated a different pattern for these nutrients. The NA-box is a region
655 that comprises part of the subtropical and subpolar gyres, and where a number of different
656 biogeochemical provinces coexist (Reygondeau et al., 2013). Hence, changes in relative
657 abundances of the non-siliceous phytoplankton (requiring nitrate and phosphate but not
658 silicate) and diatom phytoplankton communities (which in addition to phosphate and
659 nitrate require silicate) might partly explain the differential response observed in the
660 silicate vs nitrate and phosphate budgets.

661 We now split the inventories into upper/lower MOC limbs to better understand the
662 observed imbalances and their interpretation, as well as to further understand the
663 differences between the 2004 and 2010 total nutrient budgets.

664 The upper limb of the MOC within the NA-box domain was unequivocally characterized
665 by a net positive balance of inorganic nutrients (B^{uMOC}>0; Figure 5e,h,k). Under steady-
666 state conditions, this excess of nutrients should be entirely accounted for by the biological
667 term, that is, the upper limb being characterized by net nutrient consumption (organic

matter production exceeding remineralization). Our results also show that nutrient consumption was enhanced in 2010 (B^{uMOC}[2010]: 133 ± 29 kmol-Si s^{-1}, 144 ± 45 kmol-N s^{-1}, 9.0 ± 2.9 kmol-P s^{-1} in 2010, Figure 6e,h,k, red numbers) compared to 2004 (B^{uMOC}[2004]: 115 ± 29 kmol-Si s^{-1}, 92 ± 43 kmol-N s^{-1}, 3.3 ± 2.9 kmol-P s^{-1}; Figure 6e,h,k, blue numbers), although this enhancement was only statistically significant for the phosphate budget. To put numbers into context with the biological carbon pump, the phosphate consumption rate in the upper MOC limb, translated into carbon via stoichiometric ratios of the C:N:P:O_2=117:16:1:-170 (Anderson & Sarmiento, 1994), was enhanced by 5.7 kmol-P s^{-1}, equivalent to an increase in organic matter production of 0.25 ± 0.18 Pg-C yr^{-1} in 2010 (1.7 times the value in 2004, 0.14 Pg-C yr^{-1}). For comparison, the mean annual sea-air CO_2 flux in the North Atlantic (north of 14°N, including the Nordic Seas and portion of the Arctic) is -0.49 Pg-C yr^{-1} (Takahashi et al., 2009) of which our estimate of the anomalous 2010 uMOC nutrient budget represents up to 50%. Note, however, our indirect estimate should be taken as an upper-bound value, as we are assuming steady-state (no nutrient accumulation). Note as well the upper MOC limb is deep enough for remineralisation to take place too, so our estimate represents the net balance between consumption of "new" nutrients in the euphotic zone (transferred to depth via the BCP) and their remineralisation deeper in the water column within the upper limb.

The high-nutrient signature observed at 24.5°N in 2010 was also identifiable downstream in the North Atlantic by independent data sources (Figure 4j). The combination of a larger nutrient supply by horizontal advection with the heave of the isopycnals in the western-inner gyre (and subsequent upwelling of those nutrients to the sunlit upper ocean) (Figure 6d and 6e) altogether favoured an (immediate) biological response (enhanced primary production/nutrient consumption) in the upper ocean between 26.5-40°N (Figure 6b,c) and likely in the subpolar gyre (Henson et al., 2013). Actually, our results indicate that the missing nutrient source reported by Henson et al. (2013) may actually have had a subtropical origin. Summed up to the reported intense cooling of the upper subtropical Atlantic throughout 2010 (Cunningham et al., 2013) potentially favouring the carbon solubility pump, for which according to our results the heat divergence reduction (by 38% in 2010 compared to 2004) could have accounted for up to 40% contribution to the total

heat content decrease of -1.2 x10^{22} J reported by Cunningham et al. (2013), this study evidences boosted biological CO_2 uptake.

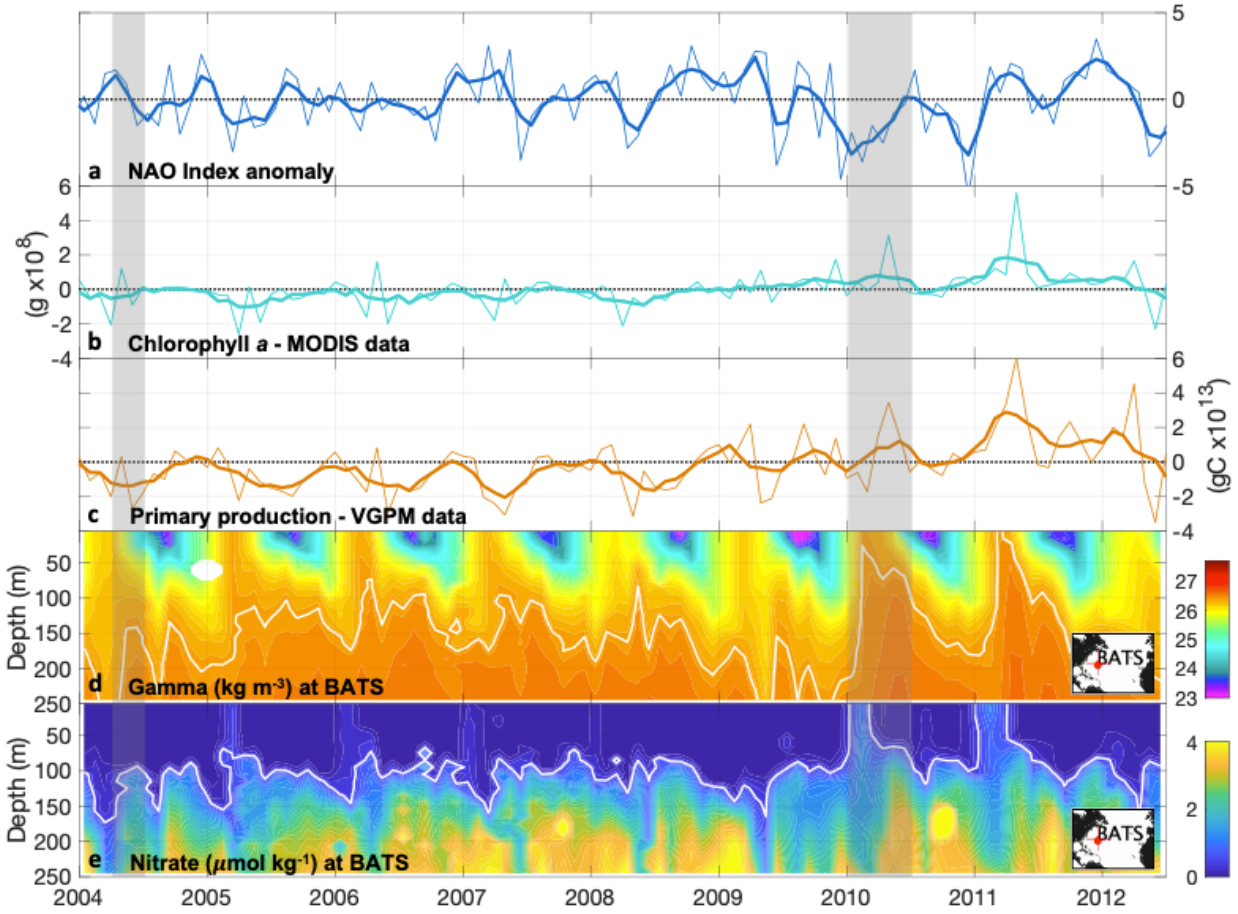

Figure 6. Time-series of a) MODIS satellite chlorophyll *a* anomalies for 25-45°N, 20-60°W box, b) MOC strength at 26.5°N, c) depth anomaly of γ_n=26.25 kg m^{-3} isopycnal at 32°N, 46°W, and e) nitrate 2004-2013 time series at the Bermuda Atlantic Time-Series (BATS) station (http://bats.bios.edu/). Bold lines in panels a to d equate to 3-month filter applied.

Conversely, the lower MOC limb was characterized by a net nutrient divergence, its magnitude exceeding the uncertainty level for silicate. For the nitrate and phosphate lower MOC budgets, we obtain net balance terms (B^{IMOC}[2004]: -69 ± 44 kmol-N s^{-1}, -3.2 ± 2.9 kmol-P s^{-1}; B^{IMOC}[2010]: -67 ± 46 kmol-N s^{-1}, -1.7 ± 3.1 kmol-P s^{-1}) consistent with organic carbon consumption at depth of about 0.19 ± 0.13 Pg-C yr^{-1} (based on the 2004 and 2010 average nitrate estimates) or 0.11 ± 0.13 Pg-C yr^{-1} (based on the 2004 and 2010 average phosphate estimates). Our estimates, although largely uncertain, can be compared with

713 the net DOC consumption rate estimated by Fontela et al. (2016) for the lower MOC limb
714 (0.062 Pg-C yr^{-1}) which would be combined with remineralisation of sinking POC.

715 Now centring the discussion in the silicate budget, we found the largest divergence of the
716 three nutrients (176 ± 76 kmol-Si s^{-1} in 2004; significantly larger in 2010, 238 ± 83 kmol-
717 Si s^{-1}). Under the steady-state assumption (no net nutrient accumulation/loss), such
718 divergence indicates net remineralization within the lower MOC limb, as might be
719 expected. In an *in situ* study in the deep northeast Atlantic (3000-m depth), Ragueneau
720 et al. (2001) estimated an annual opal flux of 43.0 mmol-Si m^{-2} yr^{-1} (i.e., 23 kmol-Si s^{-1}),
721 subject to a seasonal fluctuation between ~6 kmol-Si s^{-1} in autumn/winter to ~133 kmol-
722 Si s^{-1} in spring/summer (Ragueneau et al., 2001). When averaged with other *in situ*
723 estimates at different sites in the North Atlantic, the mean opal flux decreases to about
724 16 kmol-Si s^{-1} (0.03 mol m^{-2}, Ragueneau et al., 2000). Since most of biogenic silica
725 production is exported to deeper levels more efficiently than particulate organic carbon
726 (Segschneider & Bendtsen, 2013) and mostly recycled within the water column (Tréguer
727 et al., 1995; Loucaides et al., 2012), we could take these *in situ* measurements of opal
728 flux as a reference. Any of the *in-situ* estimates, however, are significantly lower than our
729 inferred rate. Hence, we hypothesize that the silicate divergence might actually not be
730 completely balanced by the biological remineralization term, but instead there might be
731 also a net silicate divergence in the lower MOC limb (silicate pool decreasing in time), as
732 also hypothesised in Carracedo et al. (in review). However, given the large uncertainties
733 and current limitations on the nutrient budget assessment, as well as the debateable
734 comparability between basin-scale budget and sediment-trap derived estimates, this
735 interpretation is not conclusively supported by this study, but only hypothesized.

736 *3.2.2 Further considerations on the nutrient budget estimates*

737 In this study we revisited the external nutrient sources (e.g. river runoff, atmospheric
738 input) based on the most recent studies. As illustration, the atmospheric and river runoff
739 nitrate supply used in this study (4.5 ± 4.5 kmol-N s^{-1} and 2.2 ± 0.5 kmol-N s^{-1},
740 respectively) were larger than those formerly used in the study by Álvarez et al. (2003)
741 (3.7 kmol-N $s^{-1}$and 1.4 kmol-N s^{-1}, respectively). The ongoing anthropogenic forcing is
742 very likely to keep increasing the nutrient supply via atmospheric and river runoff, as

743 evidenced by the tendency over the last few hundred years (Seitzinger et al., 2010; Moore
744 et al., 2013; Beusen et al., 2016), making them a crucial gateway by which land-based
745 human perturbations are transferred to the open ocean (Duce et al., 2008; Jickells et al.,
746 2017). However, the paucity of observations and the poor understanding of its variability
747 mean estimates remain uncertain.

748 Despite this uncertainty, one important remark is that summed up together, the external
749 nutrient sources comprise a minor term compared to the magnitude of lateral advection.
750 Hence, it is not surprising that changes in ocean circulation patterns might drive major
751 oceanic nutrient pool reorganization on interannual time-scales (this study), or multi-
752 annual – decadal timescales (Carracedo et al., in review). Climate change projections
753 predict that the MOC will decrease during the following century (IPCC Report),
754 accompanied by a general warming of the sea surface and subsequent ocean
755 stratification (Stocker et al., 2013) and, ultimately, by a reduction in primary productivity
756 (Behrenfeld et al., 2006). However, the mechanistic understanding of the regional drivers
757 at seasonal to multidecadal timescales, as well as the temporal and spatial coherences,
758 is still work in progress. Even if promising results are now being published on global ocean
759 biogeochemistry models that assimilate both physical and biogeochemical observations
760 (e.g., ECCO-Darwin; Carroll et al., 2020), adding improvement to previous non-
761 assimilation-based models (e.g. Galbraith et al., 2010; Yool et al., 2013; Stock et al., 2014;
762 Aumont et al., 2015), these are still in the evaluation phase. Therefore, observation-based
763 results can be used as benchmark for model evaluation.

764 In this study we have shown that the DWBC slowdown event in 2009/2010, which was
765 accompanied by horizontally-driven upper nutrient redistribution, actually conveyed an
766 increase in nutrient convergence in the upper MOC limb and nutrient supply to the upper
767 ocean, which ultimately favoured primary production and biological carbon uptake.
768 Therefore, under the ongoing (and projected) scenario of MOC slowdown and increasing
769 ocean stratification, extreme events injecting nutrients to the upper ocean may gain
770 relevance in boosting the biological carbon uptake in the North Atlantic.

4 Summary and conclusions

This study provided new observational basin-scale meridional nutrient transport estimates across the A05-24.5°N and OVIDE sections for the 2004 and 2010 cruises. Both sections are characterized by an upper northward (low-oxygen and low-nutrient) MOC branch carrying nutrients and oxygen to the North Atlantic, and a lower (well oxygenated and nutrient-rich) branch advecting oxygen and nutrients back to the South Atlantic. As result, this overturning pattern drives a net north-to-south meridional transport of nutrients and oxygen, so that the North Atlantic ventilates the South Atlantic and provides it with nutrients.

Lateral advection, and this upper/lower limb overturning circulation pattern, was shown as a key mechanism involved in the meridional flux of nutrients, with the Gulf Stream and its extension downstream, the North Atlantic Current, corroborated as the main advective path for the northward transfer of nutrients from low to high latitudes in the upper MOC limb; and the Deep Western Boundary Current identified as the main '*deep nutrient stream*' by the lower limb, redistributing these nutrients southwards. Although volume transport variations dominated the observed changes in the nutrient transports in most of the regions, we showed that the nutrient transport by Gulf Stream, particularly at subtropical latitudes, was also greatly influenced by changes in nutrient concentrations, which counteracted opposing changes in volume transport in 2010.

We highlighted in this study the relevance of assessing the varying role the upper and lower MOC limbs play in the transport of oxygen and nutrients, and more importantly the imbalance between both limbs, to better understand the magnitude and variability of the total water-column nutrient inventories.

First assuming steady-state, we estimated the inorganic nutrient budgets in the North Atlantic. Under this assumption, the convergence of nutrients in the upper MOC limb is balanced by net biological consumption, likewise net divergence of nutrients in the lower MOC limb is balanced by net biological regeneration, both consistent with a downward particle flux by the BCP within the region. However, our results showed *higher-than-in-situ* (silicate) remineralization rates in the lower MOC limb, so we suggest that the steady-state assumption may be compromised over the observational period. Even if external

nutrient sources (e.g., atmospheric input, river runoff) may become a more relevant input as anthropogenic forcing continues (e.g. by ice sheet melting, or increasing atmospheric dust supply), they still comprise a smaller magnitude term compared to lateral advection (particularly for silicate), so that circulation changing patterns are likely to dominate nutrient budget variability.

Despite the *in situ* observation-based nutrient budget estimates remain largely uncertain, a degree of interannual variability can be depicted, especially when paying attention to the split contribution to the upper and lower MOC limbs. As illustration, in 2010 we found a significant enhanced northward transport of more nutrient-rich waters by the upper MOC limb linked to a heave of isopycnals, which favoured an (immediate) biological response (enhanced nutrient -nitrate and phosphate- consumption) in the upper ocean between 26.5-40°N. As result, the water-column integrated nitrate and phosphate budgets in 2010 showed significant net biological production, pointing to the region as being autotrophic, and evidencing that extreme events in the atmospheric forcing, and subsequent ocean dynamics reorganization, are capable of driving (boosting) biological CO_2 uptake.

In summary, we showed that the *de facto* steady-state assumption may not be the best representation of the biogeochemical budgets, which may actually be responding on interannual time scales to circulation changes with either accumulation/depletion of the nutrient inventories in response to an excess of nutrient convergence/divergence. However, the large uncertainties associated with the nutrient sources, transports and budgets preclude an irrefutable conclusion. Therefore, we strongly encourage further research to be directed in better resolving the feedbacks between the changes in global circulation patterns and their impact on carbon and nutrient inventories in the ocean, as well as to better quantify the magnitude and variability of the external nutrient sources.

Acknowledgments, Samples, and Data

This study is a contribution to OVIDE (co-funded by the IFREMER, CNRS/INSU/LEFE), AtlantOS (EU Horizon 2020 grant No 516 633211), CLASS (NERC National Capability Science Single Centre awards), and ABC-Fluxes (NERC-funded grant No NE/M005046/1) projects. This study was supported by the TRIATLAS project, which has received funding from the European Union's Horizon 2020 research and innovation

programme under grant agreement No 817578. L.I.C. was first supported by the University of Vigo through the Galician I2C Plan for postdoctoral research, afterwards funded by NERC within the framework of the ABC-Fluxes Project. H.M. was financed by CNRS; E.M., R.S. and P.B. by NERC and NORCE; G.R. by the University of Vigo; S.T. by AWI; C.M.M. by the NERC; P.L. by IFREMER; and F.F.P. by the BOCATS2 Project (PID2019-104279GB-C21) co-funded by the Spanish Government and the FEDER, and by the project COMFORT funded from the European Union's Horizon 2020 research and innovation program under grant agreement No 820989. The authors are grateful to the captains, crew, technicians and scientists who contributed to the acquisition, processing, and quality control of the hydrographic data used in this study. We particularly thank P. Zunino for her valuable contribution to the OVIDE data interpolation. We also thank the programs that made cruise data available: GO-SHIP (www.go-ship.org), CLIVAR (www.clivar.org) and CCHDO (cchdo.ucsd.edu). Florida Current absolute transports are also available online (www.aoml.noaa.gov/phod/floridacurrent), and well as Florida Straits repeated hydrography (ftp://ftp.aoml.noaa.gov/phod/pub/WBTS/WaltonSmith/).

References

Álvarez, M., Bryden, H., Pérez, F. F., Ríos, A. F., & Rosón, G. (2002). Physical and biogeochemical fluxes and net budgets in the subpolar and temperate North Atlantic. *Journal of Marine Research*, *60*, 191–226. https://doi.org/10.1357/00222400260497462

Álvarez, M., Ríos, A. F., Pérez, F. F., Bryden, H., & Rosón, G. (2003). Transports and budgets of total inorganic carbon in the subpolar and temperate North Atlantic. *Global Biogeochemical Cycles*, *17*(1), 1002. https://doi.org/10.1029/2002GB001881

Álvarez, M., Pérez, F. F., Bryden, H., & Ríos, A. F. (2004). Physical and biogeochemical transports structure in the North Atlantic subpolar gyre. *Journal of Geophysical Research*, *109*(C3). https://doi.org/10.1029/2003JC002015

Aminot, A., & Chaussepied, M. (1983). *Manuel des analyses chimiques en Milieu Marin*. Publications du CNEXO, 395p.

Anderson, L. A., & Sarmiento, J. L. (1994). Redfield ratios of remineralization determined by nutrient data analysis. *Global Biogeochemical Cycles*, *8*(1), 65–80. https://doi.org/10.1029/93GB03318

Atkinson, C. P., Bryden, H. L., Cunningham, S. A., & King, B. A. (2012). Atlantic transport variability at 25° N in six hydrographic sections. *Ocean Science*, *8*(4), 497–523. https://doi.org/10.5194/os-8-497-2012

Atlas, R., Hoffman, R. N., Ardizzone, J., Leidner, S. M., Jusem, J. C., Smith, D. K., & Gombos, D. (2011). A Cross-calibrated, Multiplatform Ocean Surface Wind Velocity Product for Meteorological and Oceanographic Applications. *Bulletin of the American Meteorological Society*, *92*(2), 157–174. https://doi.org/10.1175/2010BAMS2946.1

Aumont, O., Ethé, C., Tagliabue, A., Bopp, L., & Gehlen, M. (2015). PISCES-v2: an ocean biogeochemical model for carbon and ecosystem studies. *Geoscientific Model Development*, *8*(8), 2465–2513.

Baringer, M. O., & Larsen, J. C. (2001). Sixteen years of Florida Current Transport at 27° N. *Geophysical Research Letters*, *28*(16), 3179–3182. https://doi.org/10.1029/2001GL013246

Benavides, M., & Voss, M. (2015). Five decades of N_2 fixation research in the North Atlantic Ocean. *Frontiers in Marine Science*, *2*, 40. https://doi.org/10.3389/fmars.2015.00040

Benavides, M., Bronk, D. A., Agawin, N. S. R., Pérez-Hernández, M. D., Hernández-Guerra, A., & Arístegui, J. (2013). Longitudinal variability of size-fractionated N2 fixation and DON release rates along 24.5°N in the subtropical North Atlantic. *Journal of Geophysical Research: Oceans*, *118*(7), 3406–3415. https://doi.org/10.1002/jgrc.20253

Beusen, A. H. W., Bouwman, A. F., Van Beek, L. P. H., Mogollón, J. M., & Middelburg, J. J. (2016). Global riverine N and P transport to ocean increased during the 20th century despite increased retention along the aquatic continuum. *Biogeosciences*, *13*(8), 2441–2451. https://doi.org/10.5194/bg-13-2441-2016

Bopp, L., Le Quéré, C., Heimann, M., Manning, A. C., & Monfray, P. (2002). Climate-induced oceanic oxygen fluxes: Implications for the contemporary carbon budget: OCEANIC O 2 FLUXES 1860-2100. *Global Biogeochemical Cycles*, *16*(2), 6-1-6–13. https://doi.org/10.1029/2001GB001445

Brown, P. J., Bakker, D. C. E., Schuster, U., & Watson, A. J. (2010). Anthropogenic carbon accumulation in the subtropical North Atlantic. *Journal of Geophysical Research: Oceans*, *115*(C4), C04016. https://doi.org/10.1029/2008JC005043

Bryden, H. L., King, B. A., McCarthy, G. D., & McDonagh, E. L. (2014). Impact of a 30% reduction in Atlantic meridional overturning during 2009/2010. *Ocean Science*, *10*(4), 683–691. https://doi.org/10.5194/os-10-683-2014

Carpenter, E. J., & Capone, D. G. (2013). *Nitrogen in the Marine Environment*. Elsevier.

Carracedo, L.I., McDonagh, E., Sanders, R., Moore, C.M., Brown, P., Torres-Valdés, S., Baringer, M., Smeed, D., & Rosón, G. (in review). Overturning circulation regulates efficiency of North Atlantic biological carbon pump.

Carroll, D., Menemenlis, D., Adkins, J. F., Bowman, K. W., Brix, H., Dutkiewicz, S., et al. (2020). The ECCO-Darwin Data-Assimilative Global Ocean Biogeochemistry Model: Estimates of Seasonal to Multidecadal Surface Ocean pCO_2 and Air-Sea CO_2 Flux. *Journal of Advances in Modeling Earth Systems*, *12*(10), e2019MS001888. https://doi.org/10.1029/2019MS001888

Chaudhuri, A. H., Gangopadhyay, A., & Bisagni, J. J. (2011). Contrasting Response of the Eastern and Western North Atlantic Circulation to an Episodic Climate Event*. *Journal of Physical Oceanography*, *41*(9), 1630–1638.

Cianca, A., Helmke, P., Mouriño, B., Rueda, M. J., Llinás, O., & Neuer, S. (2007). Decadal analysis of hydrography and in situ nutrient budgets in the western and eastern North Atlantic subtropical gyre. *Journal of Geophysical Research*, *112*(C7). https://doi.org/10.1029/2006JC003788

Culberson, C. H. (1991). *WOCE operations manual (WHP operations and methods), WHPO 91/1*. Woods Hole Oceanogr. Inst., Woods Hole, Mass.

Cunningham, S. A., Roberts, C. D., Frajka-Williams, E., Johns, W. E., Hobbs, W., Palmer, M. D., et al. (2013). Atlantic Meridional Overturning Circulation slowdown cooled the subtropical ocean: COOLING IN THE SUBTROPICAL ATLANTIC. *Geophysical Research Letters*, *40*(23), 6202–6207. https://doi.org/10.1002/2013GL058464

Curry, B., Lee, C. M., Petrie, B., Moritz, R. E., & Kwok, R. (2014). Multiyear Volume, Liquid Freshwater, and Sea Ice Transports through Davis Strait, 2004–10. *Journal of Physical Oceanography*, *44*(4), 1244–1266. https://doi.org/10.1175/JPO-D-13-0177.1

914 Daniault, N., Mercier, H., Lherminier, P., Sarafanov, A., Falina, A., Zunino, P., et al. (2016). The northern
915 North Atlantic Ocean mean circulation in the early 21st century. *Progress in Oceanography*, *146*,
916 142–158. https://doi.org/10.1016/j.pocean.2016.06.007

917 Dave, A. C., Barton, A. D., Lozier, M. S., & McKinley, G. A. (2015). What drives seasonal change in
918 oligotrophic area in the subtropical North Atlantic? *Journal of Geophysical Research: Oceans*,
919 *120*(6), 3958–3969. https://doi.org/10.1002/2015JC010787

920 Dee, D. P., Uppala, S. M., Simmons, A. J., Berrisford, P., Poli, P., Kobayashi, S., et al. (2011). The ERA-
921 Interim reanalysis: configuration and performance of the data assimilation system. *Quarterly*
922 *Journal of the Royal Meteorological Society*, *137*(656), 553–597. https://doi.org/10.1002/qj.828

923 Desbruyères, D., Thierry, V., & Mercier, H. (2013). Simulated decadal variability of the meridional
924 overturning circulation across the A25-Ovide section: Decadal variability of meridional overturning
925 circulation. *Journal of Geophysical Research: Oceans*, *118*(1), 462–475.
926 https://doi.org/10.1029/2012JC008342

927 DeVries, T., Holzer, M., & Primeau, F. (2017). Recent increase in oceanic carbon uptake driven by
928 weaker upper-ocean overturning. *Nature*, *542*(7640), 215–218.
929 https://doi.org/10.1038/nature21068

930 Duce, R. A., LaRoche, J., Altieri, K., Arrigo, K. R., Baker, A. R., Capone, D. G., et al. (2008). Impacts of
931 Atmospheric Anthropogenic Nitrogen on the Open Ocean. *Science*, *320*(5878), 893–897.
932 https://doi.org/10.1126/science.1150369

933 Dürr, H. H., Meybeck, M., Hartmann, J., Laruelle, G. G., & Roubeix, V. (2011). Global spatial distribution
934 of natural riverine silica inputs to the coastal zone. *Biogeosciences*, *8*(3), 597–620.
935 https://doi.org/10.5194/bg-8-597-2011

936 Emerson, S., Mecking, S., & Abell, J. (2001). The biological pump in the subtropical North Pacific Ocean:
937 Nutrient sources, Redfield ratios, and recent changes. *Global Biogeochemical Cycles*, *15*(3),
938 535–554. https://doi.org/10.1029/2000GB001320

939 Falkowski, P. G., Barber, R. T., & Smetacek, V. (1998). Biogeochemical Controls and Feedbacks on
940 Ocean Primary Production. *Science*, *281*(5374), 200–206.
941 https://doi.org/10.1126/science.281.5374.200

942 Fontela, M., García-Ibáñez, M. I., Hansell, D. A., Mercier, H., & Pérez, F. F. (2016). Dissolved Organic
943 Carbon in the North Atlantic Meridional Overturning Circulation. *Scientific Reports*, *6*, 26931.
944 https://doi.org/10.1038/srep26931

945 Fontela, M., Mercier, H., & Pérez, F. F. (2019). Long-term integrated biogeochemical budget driven by
946 circulation in the eastern subpolar North Atlantic. *Progress in Oceanography*.
947 https://doi.org/10.1016/j.pocean.2019.02.004

948 Fratantoni, P. S., & McCartney, M. S. (2010). Freshwater export from the Labrador Current to the North
949 Atlantic Current at the Tail of the Grand Banks of Newfoundland. *Deep Sea Research Part I:*
950 *Oceanographic Research Papers*, *57*(2), 258–283. https://doi.org/10.1016/j.dsr.2009.11.006

951 Fröb, F., Olsen, A., Våge, K., Moore, G. W. K., Yashayaev, I., Jeansson, E., & Rajasakaren, B. (2016).
952 Irminger Sea deep convection injects oxygen and anthropogenic carbon to the ocean interior.
953 *Nature Communications*, *7*, 13244. https://doi.org/10.1038/ncomms13244

954 Galbraith, E. D., Gnanadesikan, A., Dunne, J. P., & Hiscock, M. R. (2010). Regional impacts of iron-light
955 colimitation in a global biogeochemical model. *Biogeosciences*, *7*(3), 1043–1064.
956 https://doi.org/10.5194/bg-7-1043-2010

957 Ganachaud, A., & Wunsch, C. (2002). Oceanic nutrient and oxygen transports and bounds on export
958 production during the World Ocean Circulation Experiment. *Global Biogeochemical Cycles*, *16*(4),
959 5-1-5–14. https://doi.org/10.1029/2000GB001333

960 Ganachaud, A. (2003). Error budget of inverse box models: The North Atlantic. *Journal of Atmospheric*
961 *and Oceanic Technology*, *20*(11), 1641–1655.

962 Garcia, H., Cruzado, A., Gordon, L., & Escanez, J. (1998). Decadal-scale chemical variability in the
963 subtropical North Atlantic deduced from nutrient and oxygen data. *Journal of Geophysical*
964 *Research: Oceans*, *103*(C2), 2817–2830. https://doi.org/10.1029/97JC03037

965 García, H., Boyer, T. P., Levitus, S., Locarnini, R. A., & Antonov, J. (2005). On the variability of dissolved
966 oxygen and apparent oxygen utilization content for the upper world ocean: 1955 to 1998.
967 *Geophysical Research Letters*, *32*(9), L09604. https://doi.org/10.1029/2004GL022286

968 García-Ibáñez, M. I., Pardo, P. C., Carracedo, L. I., Mercier, H., Lherminier, P., Ríos, A. F., & Pérez, F. F.
969 (2015). Structure, transports and transformations of the water masses in the Atlantic Subpolar
970 Gyre. *Progress in Oceanography*, *135*, 18–36. https://doi.org/10.1016/j.pocean.2015.03.009

971 Gruber, N., & Sarmiento, J. L. (1997). Global patterns of marine nitrogen fixation and denitrification.
972 *Global Biogeochemical Cycles*, *11*(2), 235–266. https://doi.org/10.1029/97GB00077

973 Gruber, N., Gloor, M., Fan, S.-M., & Sarmiento, J. L. (2001). Air-sea flux of oxygen estimated from bulk
974 data: Implications For the marine and atmospheric oxygen cycles. *Global Biogeochemical Cycles*,
975 *15*(4), 783–803. https://doi.org/10.1029/2000GB001302

976 Gruber, N., Clement, D., Carter, B. R., Feely, R. A., Heuven, S. van, Hoppema, M., et al. (2019). The
977 oceanic sink for anthropogenic CO2 from 1994 to 2007. *Science*, *363*(6432), 1193–1199.
978 https://doi.org/10.1126/science.aau5153

979 Guallart, E. F., Schuster, U., Fajar, N. M., Legge, O., Brown, P., Pelejero, C., et al. (2015). Trends in
980 anthropogenic CO_2 in water masses of the Subtropical North Atlantic Ocean. *Progress in*
981 *Oceanography*, *131*, 21–32. https://doi.org/10.1016/j.pocean.2014.11.006

982 Hansell, D. A., & Follows, M. J. (2008). Chapter 13 - Nitrogen in the Atlantic Ocean. In *Nitrogen in the*
983 *Marine Environment (2nd Edition)* (pp. 597–630). San Diego: Academic Press.
984 https://doi.org/10.1016/B978-0-12-372522-6.00013-X

985 Hansell, D. A., Carlson, C. A., Repeta, D. J., & Schlitzer, R. (2009). Dissolved organic matter in the
986 ocean: A controversy stimulates new insights. *Oceanography*, *22*(4), 202–211.

987 Hawkings, J. R., Wadham, J. L., Benning, L. G., Hendry, K. R., Tranter, M., Tedstone, A., et al. (2017).
988 Ice sheets as a missing source of silica to the polar oceans. *Nature Communications*, *8*, 14198.
989 https://doi.org/10.1038/ncomms14198

990 Heinze, C., Meyer, S., Goris, N., Anderson, L., Steinfeldt, R., Chang, N., et al. (2015). The ocean carbon
991 sink – impacts, vulnerabilities and challenges. *Earth System Dynamics*, *6*(1), 327–358.
992 https://doi.org/10.5194/esd-6-327-2015

993 Henson, S. A., Painter, S. C., Penny Holliday, N., Stinchcombe, M. C., & Giering, S. L. C. (2013). Unusual
994 subpolar North Atlantic phytoplankton bloom in 2010: Volcanic fertilization or North Atlantic
995 Oscillation? *Journal of Geophysical Research: Oceans*, *118*(10), 4771–4780.
996 https://doi.org/10.1002/jgrc.20363

997 Hernández-Guerra, A., Pelegrí, J. L., Fraile-Nuez, E., Benítez-Barrios, V., Emelianov, M., Pérez-
998 Hernández, M. D., & Vélez-Belchí, P. (2014). Meridional overturning transports at 7.5N and 24.5N
999 in the Atlantic Ocean during 1992–93 and 2010–11. *Progress in Oceanography*, *128*, 98–114.
1000 https://doi.org/10.1016/j.pocean.2014.08.016

1001 Holliday, N. P., Bacon, S., Cunningham, S. A., Gary, S. F., Karstensen, J., King, B. A., et al. (2018).
1002 Subpolar North Atlantic Overturning and Gyre-Scale Circulation in the Summers of 2014 and
1003 2016. *Journal of Geophysical Research: Oceans*, *123*(7), 4538–4559.
1004 https://doi.org/10.1029/2018JC013841

1005 Huertas, I. E., Ríos, A. F., García-Lafuente, J., Navarro, G., Makaoui, A., Sánchez-Román, A., et al.
1006 (2012). Atlantic forcing of the Mediterranean oligotrophy. *Global Biogeochemical Cycles*, *26*(2),
1007 n/a-n/a. https://doi.org/10.1029/2011GB004167

1008 Hurrell J. W., Kushnir Y., Ottersen G., & Visbeck M. (2013). An Overview of the North Atlantic Oscillation.
1009 *The North Atlantic Oscillation: Climatic Significance and Environmental Impact*.
1010 https://doi.org/10.1029/134GM01

1011 Ito, T., & Follows, M. J. (2005). Preformed phosphate, soft tissue pump and atmospheric CO2. *Journal of*
1012 *Marine Research*, *63*(4), 813–839.

1013 Jickells, T. D., Buitenhuis, E., Altieri, K., Baker, A. R., Capone, D., Duce, R. A., et al. (2017). A
1014 reevaluation of the magnitude and impacts of anthropogenic atmospheric nitrogen inputs on the
1015 ocean. *Global Biogeochemical Cycles*, *31*(2), 2016GB005586.
1016 https://doi.org/10.1002/2016GB005586

1017 Kanzow, T., Cunningham, S. A., Johns, W. E., Hirschi, J. J.-M., Marotzke, J., Baringer, M. O., et al.
1018 (2010). Seasonal Variability of the Atlantic Meridional Overturning Circulation at 26.5°N. *Journal*
1019 *of Climate*, *23*(21), 5678–5698. https://doi.org/10.1175/2010JCLI3389.1

1020 Khatiwala, S., Tanhua, T., Mikaloff Fletcher, S., Gerber, M., Doney, S. C., Graven, H. D., et al. (2013).
1021 Global ocean storage of anthropogenic carbon. *Biogeosciences*, *10*(4), 2169–2191.
1022 https://doi.org/10.5194/bg-10-2169-2013

1023 Kirkwood, D. (1996). *Nutrients: Practical Notes on Their Determination in Sea Water*. International
1024 Council for the Exploration of the Sea.

1025 Kistler, R., Kalnay, E., Collins, W., Saha, S., White, G., Woollen, J., et al. (2001). The NCEP–NCAR 50-
1026 Year Reanalysis: Monthly Means CD-ROM and Documentation. *Bulletin of the American*
1027 *Meteorological Society*, *82*(2), 247–268. https://doi.org/10.1175/1520-
1028 0477(2001)082<0247:TNNYRM>2.3.CO;2

1029 Langdon, C. (2010). Determination of Dissolved Oxygen in Seawater by Winkler Titration Using The
1030 Amperometric Technique. Retrieved from
1031 https://repository.oceanbestpractices.org/handle/11329/380

1032 Lavín, A. M., Bryden, H. L., & Parrilla, G. (2003). Mechanisms of heat, freshwater, oxygen and nutrient
1033 transports and budgets at 24.5°N in the subtropical North Atlantic. *Deep Sea Research Part I:*
1034 *Oceanographic Research Papers*, *50*(9), 1099–1128. https://doi.org/10.1016/S0967-
1035 0637(03)00095-5

1036 Letscher, R. T., Hansell, D. A., Carlson, C. A., Lumpkin, R., & Knapp, A. N. (2013). Dissolved organic
1037 nitrogen in the global surface ocean: Distribution and fate. *Global Biogeochemical Cycles*, *27*(1),
1038 141–153. https://doi.org/10.1029/2012GB004449

1039 Letscher, R. T., Primeau, F., & Moore, J. K. (2016). Nutrient budgets in the subtropical ocean gyres
1040 dominated by lateral transport. *Nature Geoscience*, *9*(11), 815–819.
1041 https://doi.org/10.1038/ngeo2812

1042 Lherminier, P., Mercier, H., Gourcuff, C., Alvarez, M., Bacon, S., & Kermabon, C. (2007). Transports
1043 across the 2002 Greenland-Portugal Ovide section and comparison with 1997. *Journal of*
1044 *Geophysical Research*, *112*(C7), C07003.

1045 Lherminier, P., Mercier, H., Huck, T., Gourcuff, C., Perez, F. F., Morin, P., et al. (2010). The Atlantic
1046 Meridional Overturning Circulation and the subpolar gyre observed at the A25-OVIDE section in
1047 June 2002 and 2004. *Deep Sea Research Part I: Oceanographic Research Papers*, *57*(11),
1048 1374–1391. https://doi.org/10.1016/j.dsr.2010.07.009

1049 Loucaides, S., Cappellen, P. V., Roubeix, V., Moriceau, B., & Ragueneau, O. (2012). Controls on the
1050 Recycling and Preservation of Biogenic Silica from Biomineralization to Burial. *Silicon*, *4*(1), 7–22.
1051 https://doi.org/10.1007/s12633-011-9092-9

1052 Mahaffey, C., Williams, R. G., Wolff, G. A., & Anderson, W. T. (2004). Physical supply of nitrogen to
1053 phytoplankton in the Atlantic Ocean. *Global Biogeochemical Cycles*, *18*(1).
1054 https://doi.org/10.1029/2003GB002129

1055 Mahowald, N., Jickells, T. D., Baker, A. R., Artaxo, P., Benitez-Nelson, C. R., Bergametti, G., et al.
1056 (2008). Global distribution of atmospheric phosphorus sources, concentrations and deposition
1057 rates, and anthropogenic impacts. *Global Biogeochemical Cycles*, *22*(4), GB4026.
1058 https://doi.org/10.1029/2008GB003240

1059 Martel, F., & Wunsch, C. (1993). The North Atlantic Circulation in the Early 1980s-An Estimate from
1060 Inversion of a Finite-Difference Model. *Journal of Physical Oceanography*, *23*(5), 898–924.
1061 https://doi.org/10.1175/1520-0485(1993)023<0898:TNACIT>2.0.CO;2

1062 Matear, R. J., & Hirst, A. C. (2003). Long-term changes in dissolved oxygen concentrations in the ocean
1063 caused by protracted global warming. *Global Biogeochemical Cycles*, *17*(4), 1125.
1064 https://doi.org/10.1029/2002GB001997

1065 Mather, R. L., Reynolds, S. E., Wolff, G. A., Williams, R. G., Torres-Valdes, S., Woodward, E. M. S., et al.
1066 (2008). Phosphorus cycling in the North and South Atlantic Ocean subtropical gyres. *Nature*
1067 *Geoscience*, *1*(7), 439–443. https://doi.org/10.1038/ngeo232

1068 Mayorga, E., Seitzinger, S. P., Harrison, J. A., Dumont, E., Beusen, A. H. W., Bouwman, A. F., et al.
1069 (2010). Global Nutrient Export from WaterSheds 2 (NEWS 2): Model development and
1070 implementation. *Environmental Modelling & Software*, *25*(7), 837–853.
1071 https://doi.org/10.1016/j.envsoft.2010.01.007

1072 Maze, G., Mercier, H., Thierry, V., Memery, L., Morin, P., & Perez, F. F. (2012). Mass, nutrient and
1073 oxygen budgets for the northeastern Atlantic Ocean. *Biogeosciences*, *9*(10), 4099–4113.
1074 https://doi.org/10.5194/bg-9-4099-2012

1075 McCarthy, G., Frajka-Williams, E., Johns, W. E., Baringer, M. O., Meinen, C. S., Bryden, H. L., et al.
1076 (2012). Observed interannual variability of the Atlantic meridional overturning circulation at
1077 26.5°N: Interannual variability of the MOC. *Geophysical Research Letters*, *39*(19), n/a-n/a.
1078 https://doi.org/10.1029/2012GL052933

1079 McCarthy, G. D., Smeed, D. A., Johns, W. E., Frajka-Williams, E., Moat, B. I., Rayner, D., et al. (2015).
1080 Measuring the Atlantic Meridional Overturning Circulation at 26°N. *Progress in Oceanography*,
1081 *130*, 91–111. https://doi.org/10.1016/j.pocean.2014.10.006

1082 McDonagh, E. L., King, B. A., Bryden, H. L., Courtois, P., Szuts, Z., Baringer, M., et al. (2015).
1083 Continuous Estimate of Atlantic Oceanic Freshwater Flux at 26.5°N. *Journal of Climate*, *28*(22),
1084 8888–8906. https://doi.org/10.1175/JCLI-D-14-00519.1

1085 Meinen, C. S., Garzoli, S. L., Johns, W. E., & Baringer, M. O. (2004). Transport variability of the Deep
1086 Western Boundary Current and the Antilles Current off Abaco Island, Bahamas. *Deep Sea*
1087 *Research Part I: Oceanographic Research Papers*, *51*(11), 1397–1415.
1088 https://doi.org/10.1016/j.dsr.2004.07.007

1089 Meinen, C. S., Baringer, M. O., & Garcia, R. F. (2010). Florida Current transport variability: An analysis of
1090 annual and longer-period signals. *Deep Sea Research Part I: Oceanographic Research Papers*,
1091 *57*(7), 835–846. https://doi.org/10.1016/j.dsr.2010.04.001

1092 Mercier, H. (1986). Determining the general circulation of the ocean: A nonlinear inverse problem. *Journal*
1093 *Of Geophysical Research Oceans*, *91*(C4), 5103–5109.

1094 Mercier, H. Lherminier, P., Sarafanov, A., Gaillard, F., Daniault, N., Desbruyères, D., et al. (2015).
1095 Variability of the meridional overturning circulation at the Greenland–Portugal OVIDE section from
1096 1993 to 2010. *Progress in Oceanography*, *132*, 250–261.
1097 https://doi.org/10.1016/j.pocean.2013.11.001

1098 Michaels, A. F., Olson, D., Sarmiento, J. L., Ammerman, J. W., Fanning, K., Jahnke, R., et al. (1996).
1099 Inputs, losses and transformations of nitrogen and phosphorus in the pelagic North Atlantic
1100 Ocean. *Biogeochemistry*, *35*(1), 181–226. https://doi.org/10.1007/BF02179827

1101 Moore, C. M., Mills, M. M., Arrigo, K. R., Berman-Frank, I., Bopp, L., Boyd, P. W., et al. (2013). Processes
1102 and patterns of oceanic nutrient limitation. *Nature Geosci*, *6*(9), 701–710.

1103 Olsen, A., Lange, N., Key, R. M., Tanhua, T., Álvarez, M., Becker, S., et al. (2019). GLODAPv2.2019 – an
1104 update of GLODAPv2. *Earth System Science Data*, *11*(3), 1437–1461.
1105 https://doi.org/10.5194/essd-11-1437-2019

1106 Osborn, T. J. (2011). Winter 2009/2010 temperatures and a record-breaking North Atlantic Oscillation
1107 index. *Weather*, *66*(1), 19–21. https://doi.org/10.1002/wea.660

1108 Oschlies, A. (2001). NAO-induced long-term changes in nutrient supply to the surface waters of the North
1109 Atlantic. *Geophysical Research Letters*, *28*(9), 1751–1754.
1110 https://doi.org/10.1029/2000GL012328

1111 Palter, J. B., Lozier, M. S., & Barber, R. T. (2005). The effect of advection on the nutrient reservoir in the
1112 North Atlantic subtropical gyre. *Nature*, *437*(7059), 687–692. https://doi.org/10.1038/nature03969

1113 Palter, J. B., Lozier, M. S., Sarmiento, J. L., & Williams, R. G. (2011). The supply of excess phosphate
1114 across the Gulf Stream and the maintenance of subtropical nitrogen fixation. *Global*
1115 *Biogeochemical Cycles*, *25*(4). https://doi.org/10.1029/2010GB003955

1116 Pelegrí, J. L., & Csanady, G. T. (1991). Nutrient transport and mixing in the Gulf Stream. *Journal of*
1117 *Geophysical Research: Oceans*, *96*(C2), 2577–2583. https://doi.org/10.1029/90JC02535

1118 Pelegrí, J. L., Marrero-Díaz, A., & Ratsimandresey, A. W. (2006). Nutrient irrigation of the North Atlantic.
1119 *Progress in Oceanography*, *70*(2–4), 366–406. https://doi.org/10.1016/j.pocean.2006.03.018

1120 Pérez, F. F., Gilcoto, M., & Ríos, A. F. (2003). Large and mesoscale variability of the water masses and
1121 the deep chlorophyll maximum in the Azores Front. *Journal of Geophysical Research*, *108*(C7),
1122 3215. https://doi:10.1029/2000JC000360.

1123 Peucker-Ehrenbrink, B. (2009). Land2Sea database of river drainage basin sizes, annual water
1124 discharges, and suspended sediment fluxes. *Geochemistry, Geophysics, Geosystems*, *10*(6).
1125 https://doi.org/10.1029/2008GC002356

1126 Pommier, J., Gosselin, M., & Michel, C. (2009). Size-fractionated phytoplankton production and biomass
1127 during the decline of the northwest Atlantic spring bloom. *Journal of Plankton Research*, *31*(4),
1128 429–446. https://doi.org/10.1093/plankt/fbn127

1129 Racapé, V., Zunino, P., Mercier, H., Lherminier, P., Bopp, L., Pérèz, F. F., & Gehlen, M. (2018). Transport
1130 and storage of anthropogenic C in the North Atlantic Subpolar Ocean. *Biogeosciences*, *15*(14),
1131 4661–4682. https://doi.org/10.5194/bg-15-4661-2018

1132 Ragueneau, O., Tréguer, P., Leynaert, A., Anderson, R. F., Brzezinski, M. A., DeMaster, D. J., et al.
1133 (2000). A review of the Si cycle in the modern ocean: recent progress and missing gaps in the
1134 application of biogenic opal as a paleoproductivity proxy. *Global and Planetary Change*, *26*(4),
1135 317–365. https://doi.org/10.1016/S0921-8181(00)00052-7

1136 Ragueneau, O., Gallinari, M., Corrin, L., Grandel, S., Hall, P., Hauvespre, A., et al. (2001). The benthic
1137 silica cycle in the Northeast Atlantic: annual mass balance, seasonality, and importance of non-
1138 steady-state processes for the early diagenesis of biogenic opal in deep-sea sediments. *Progress*
1139 *in Oceanography*, *50*(1), 171–200. https://doi.org/10.1016/S0079-6611(01)00053-2

1140 Reygondeau, G., Longhurst, A., Martinez, E., Beaugrand, G., Antoine, D., & Maury, O. (2013). Dynamic
1141 biogeochemical provinces in the global ocean. *Global Biogeochemical Cycles*, *27*(4), 1046–1058.
1142 https://doi.org/10.1002/gbc.20089

1143 Reynolds, S., Mahaffey, C., Roussenov, V., & Williams, R. G. (2014). Evidence for production and lateral
1144 transport of dissolved organic phosphorus in the eastern subtropical North Atlantic. *Global*
1145 *Biogeochemical Cycles*, *28*(8), 805–824. https://doi.org/10.1002/2013GB004801

1146 Rintoul, S. R., & Wunsch, C. (1991). Mass, heat, oxygen and nutrient fluxes and budgets in the North
1147 Atlantic Ocean. *Deep Sea Research Part A. Oceanographic Research Papers*, *38*, S355–S377.
1148 https://doi.org/10.1016/S0198-0149(12)80017-3

1149 Roussenov, V., Williams, R. G., Mahaffey, C., & Wolff, G. A. (2006). Does the transport of dissolved
1150 organic nutrients affect export production in the Atlantic Ocean? *Global Biogeochemical Cycles*,
1151 *20*(3). https://doi.org/10.1029/2005GB002510

1152 Sarafanov, A. (2009). On the effect of the North Atlantic Oscillation on temperature and salinity of the
1153 subpolar North Atlantic intermediate and deep waters. *ICES Journal of Marine Science: Journal*
1154 *Du Conseil*, *66*(7), 1448–1454.

1155 Schlitzer, R. (1988). Modeling the nutrient and carbon cycles of the North Atlantic: 1. Circulation, mixing
1156 coefficients, and heat fluxes. *Journal of Geophysical Research: Oceans*, *93*(C9), 10699–10723.
1157 https://doi.org/10.1029/JC093iC09p10699

1158 Segschneider, J., & Bendtsen, J. (2013). Temperature-dependent remineralization in a warming ocean
1159 increases surface pCO_2 through changes in marine ecosystem composition. *Global*
1160 *Biogeochemical Cycles*, *27*(4), 2013GB004684. https://doi.org/10.1002/2013GB004684

1161 Seitzinger, S. P., Mayorga, E., Bouwman, A. F., Kroeze, C., Beusen, A. H. W., Billen, G., et al. (2010).
1162 Global river nutrient export: A scenario analysis of past and future trends. *Global Biogeochemical*
1163 *Cycles*, *24*(4), GB0A08. https://doi.org/10.1029/2009GB003587

1164 Serreze, M. C., Barrett, A. P., Slater, A. G., Woodgate, R. A., Aagaard, K., Lammers, R. B., et al. (2006).
1165 The large-scale freshwater cycle of the Arctic. *Journal of Geophysical Research: Oceans*,
1166 *111*(C11). https://doi.org/10.1029/2005JC003424

1167 Sharples, J., Middelburg, J. J., Fennel, K., & Jickells, T. D. (2016). What proportion of riverine nutrients
1168 reaches the open ocean? *Global Biogeochemical Cycles*, *31*(1), 2016GB005483.
1169 https://doi.org/10.1002/2016GB005483

1170 Siedler, G., Church, J., Gould, J., & Gould, W. J. (2001). *Ocean circulation and climate: observing and*
1171 *modelling the global ocean*. Academic Press.

1172 Singh, A., Lomas, M. W., & Bates, N. R. (2013). Revisiting N_2 fixation in the North Atlantic Ocean:
1173 Significance of deviations from the Redfield Ratio, atmospheric deposition and climate variability.
1174 *Deep Sea Research Part II: Topical Studies in Oceanography*, *93*, 148–158.
1175 https://doi.org/10.1016/j.dsr2.2013.04.008

1176 Smeed, D., Moat, B. I., Rayner, D., Johns, W. E., Baringer, M. O., Volkov, D. L., & Frajka-Williams, E.
1177 (2019). Atlantic meridional overturning circulation observed by the RAPID-MOCHA-WBTS array
1178 at 26N from 2004 to 2018. *British Oceanographic Data Centre*. https://doi.org/10/c72s

1179 Smeed, D. A., McCarthy, G. D., Cunningham, S. A., Frajka-Williams, E., Rayner, D., Johns, W. E., et al.
1180 (2014). Observed decline of the Atlantic meridional overturning circulation 2004-2012. *Ocean*
1181 *Science*, *10*(1), 29–38. https://doi.org/10.5194/os-10-29-2014

1182 Smeed, D. A., Josey, S. A., Beaulieu, C., Johns, W. E., Moat, B. I., Frajka-Williams, E., et al. (2018). The
1183 North Atlantic Ocean Is in a State of Reduced Overturning. *Geophysical Research Letters*, *45*(3),
1184 2017GL076350. https://doi.org/10.1002/2017GL076350

1185 Srokosz, M. A., & Bryden, H. L. (2015). Observing the Atlantic Meridional Overturning Circulation yields a
1186 decade of inevitable surprises. *Science*, *348*(6241), 1255575–1255575.
1187 https://doi.org/10.1126/science.1255575

1188 Stendardo, I., & Gruber, N. (2012). Oxygen trends over five decades in the North Atlantic. *Journal of*
1189 *Geophysical Research: Oceans*, *117*(C11), C11004. https://doi.org/10.1029/2012JC007909

1190 Stepanov, V. N., & Haines, K. (2014). Mechanisms of Atlantic Meridional Overturning Circulation
1191 variability simulated by the NEMO model. *Ocean Science*, *10*(4), 645–656.
1192 https://doi.org/10.5194/os-10-645-2014

1193 Stock, C. A., Dunne, J. P., & John, J. G. (2014). Global-scale carbon and energy flows through the
1194 marine planktonic food web: An analysis with a coupled physical–biological model. *Progress in*
1195 *Oceanography*, *120*, 1–28. https://doi.org/10.1016/j.pocean.2013.07.001

1196 Stocker, T. F., Qin, D., Plattner, G.-K., Tignor, M., Allen, S. K., Boschung, J., et al. (Eds.). (2013). *Climate*
1197 *Change 2013: The Physical Science Basis. Contribution of Working Group I to the Fifth*
1198 *Assessment Report of the Intergovernmental Panel on Climate Change*. Cambridge, United
1199 Kingdom and New York, NY, USA: Cambridge University Press. Retrieved from
1200 doi:10.1017/CBO9781107415324

1201 Stramma, L., Johnson, G. C., Sprintall, J., & Mohrholz, V. (2008). Expanding Oxygen-Minimum Zones in
1202 the Tropical Oceans. *Science*, *320*(5876), 655–658. https://doi.org/10.1126/science.1153847

1203 Stramma, L., Schmidtko, S., Levin, L. A., & Johnson, G. C. (2010). Ocean oxygen minima expansions
1204 and their biological impacts. *Deep Sea Research Part I: Oceanographic Research Papers*, *57*(4),
1205 587–595. https://doi.org/10.1016/j.dsr.2010.01.005

1206 Sutton, R. T., McCarthy, G. D., Robson, J., Sinha, B., Archibald, A. T., & Gray, L. J. (2017). Atlantic
1207 Multidecadal Variability and the U.K. ACSIS Program. *Bulletin of the American Meteorological*
1208 *Society*, *99*(2), 415–425. https://doi.org/10.1175/BAMS-D-16-0266.1

1209 Takahashi, T., Sutherland, S. C., Wanninkhof, R., Sweeney, C., Feely, R. A., Chipman, D. W., et al.
1210 (2009). Climatological mean and decadal change in surface ocean pCO_2, and net sea-air CO_2
1211 flux over the global oceans. *Deep Sea Research Part II: Topical Studies in Oceanography*, *56*(8–
1212 10), 554–577. https://doi.org/10.1016/j.dsr2.2008.12.009

1213 Talley, L. D., Pickard, G. L., Emery, W. J., & Swift, J. H. (2007). *Descriptive Physical Oceanography, Sixth*
1214 *Edition: An Introduction* (6th ed.). Academic Press.

1215 Torres-Valdés, S., Roussenov, V. M., Sanders, R., Reynolds, S., Pan, X., Mather, R., et al. (2009).
1216 Distribution of dissolved organic nutrients and their effect on export production over the Atlantic
1217 Ocean. *Global Biogeochemical Cycles*, *23*(4). https://doi.org/10.1029/2008GB003389

1218 Torres-Valdés, S., Tsubouchi, T., Bacon, S., Naveira-Garabato, A. C., Sanders, R., McLaughlin, F. A., et
1219 al. (2013). Export of nutrients from the Arctic Ocean. *Journal of Geophysical Research: Oceans*,
1220 *118*(4), 1625–1644. https://doi.org/10.1002/jgrc.20063

1221 Tréguer, P., Nelson, D. M., Van Bennekom, A. J., Demaster, D. J., Leynaert, A., & Quéguiner, B. (1995).
1222 The silica balance in the world ocean: a reestimate. *Science (New York, N.Y.)*, *268*(5209), 375–
1223 379. https://doi.org/10.1126/science.268.5209.375

1224 Tréguer, P. J., & Rocha, C. L. D. L. (2013). The World Ocean Silica Cycle. *Annual Review of Marine*
1225 *Science*, *5*(1), 477–501. https://doi.org/10.1146/annurev-marine-121211-172346

1226 Treguier, A. M., Gourcuff, C., Lherminier, P., Mercier, H., Barnier, B., Madec, G., et al. (2006). Internal
1227 and forced variability along a section between Greenland and Portugal in the CLIPPER Atlantic
1228 model. *Ocean Dynamics*, *56*(5–6), 568–580. https://doi.org/10.1007/s10236-006-0069-y

1229 Tsubouchi, T., Bacon, S., Naveira Garabato, A. C., Aksenov, Y., Laxon, S. W., Fahrbach, E., et al. (2012).
1230 The Arctic Ocean in summer: A quasi-synoptic inverse estimate of boundary fluxes and water
1231 mass transformation. *Journal of Geophysical Research: Oceans*, *117*(C1), C01024.
1232 https://doi.org/10.1029/2011JC007174

1233 Watson, A. J., Schuster, U., Bakker, D. C. E., Bates, N. R., Corbiere, A., Gonzalez-Davila, M., et al.
1234 (2009). Tracking the Variable North Atlantic Sink for Atmospheric CO_2. *Science*, *326*, 1391–1393.
1235 https://doi.org/10.1126/science.1177394

1236 Williams, R. G., & Follows, M. J. (1998). The Ekman transfer of nutrients and maintenance of new
1237 production over the North Atlantic. *Deep Sea Research Part I: Oceanographic Research Papers*,
1238 *45*(2), 461–489. https://doi.org/10.1016/S0967-0637(97)00094-0

1239 Williams, R. G., & Follows, M. J. (2003). Physical Transport of Nutrients and the Maintenance of
1240 Biological Production. In *Ocean Biogeochemistry* (pp. 19–51). Springer, Berlin, Heidelberg.
1241 https://doi.org/10.1007/978-3-642-55844-3_3

1242 Williams, R. G., McLaren, A. J., & Follows, M. J. (2000). Estimating the convective supply of nitrate and
1243 implied variability in export production over the North Atlantic. *Global Biogeochemical Cycles*,
1244 *14*(4), 1299–1313. https://doi.org/10.1029/2000GB001260

1245 Williams, R. G., Roussenov, V., & Follows, M. J. (2006). Nutrient streams and their induction into the
1246 mixed layer. *Global Biogeochemical Cycles*, *20*, GB1016. https://doi.org/10.1029/2005GB002586

1247 Williams, R. G., McDonagh, E., Roussenov, V. M., Torres-Valdes, S., King, B., Sanders, R., & Hansell, D.
1248 A. (2011). Nutrient streams in the North Atlantic: Advective pathways of inorganic and dissolved
1249 organic nutrients. *Global Biogeochemical Cycles*, *25*(4), GB4008.
1250 https://doi.org/10.1029/2010GB003853

1251 Woodgate, R. A., & Aagaard, K. (2005). Revising the Bering Strait freshwater flux into the Arctic Ocean.
1252 *Geophysical Research Letters*, *32*(2). https://doi.org/10.1029/2004GL021747

1253 Woodgate, R. A., Aagaard, K., & Weingartner, T. J. (2005). Monthly temperature, salinity, and transport
1254 variability of the Bering Strait through flow. *Geophysical Research Letters*, *32*(4).
1255 https://doi.org/10.1029/2004GL021880

1256 Yang, S., & Gruber, N. (2016). The anthropogenic perturbation of the marine nitrogen cycle by
1257 atmospheric deposition: Nitrogen cycle feedbacks and the ^{15}N Haber-Bosch effect. *Global*
1258 *Biogeochemical Cycles*, *30*(10), 1418–1440. https://doi.org/10.1002/2016GB005421

1259 Yool, A., Popova, E. E., & Anderson, T. R. (2013). MEDUSA-2.0: an intermediate complexity
1260 biogeochemical model of the marine carbon cycle for climate change and ocean acidification
1261 studies. *Geoscientific Model Development*, *6*(5), 1767–1811. https://doi.org/10.5194/gmd-6-1767-
1262 2013

1263 Zunino, P., Garcia-Ibanez, M. I., Lherminier, P., Mercier, H., Ríos, A. F., & Pérez, F. F. (2014). Variability
1264 of the transport of anthropogenic CO_2 at the Greenland-Portugal OVIDE section: controlling
1265 mechanisms. *Biogeosciences*, *11*(8), 2375–2389.

1266 Zunino, P., Pérez, F. F., Fajar, N. M., Guallart, E. F., Ríos, A. F., Pelegrí, J. L., & Hernández-Guerra, A.
1267 (2015). Transports and budgets of anthropogenic CO_2 in the tropical North Atlantic in 1992–1993
1268 and 2010–2011. *Global Biogeochemical Cycles*, *29*(7), 2014GB005075.
1269 https://doi.org/10.1002/2014GB005075

1270